Tunable Multilayer Plasmonic Materials: Optical and Topographic Characterizations

by

Jyothi Karri

B.E., Andhra University, 2006

A thesis submitted to the

Faculty of the Graduate School of the

University of Colorado in partial fulfillment

of the requirements for the degree of

Master of Sciences

Department of Electrical Computer and Energy Engineering

2011

This thesis entitled:
Tunable Multilayer Plasmonic Materials: Optical and Topographic Characterizations
written by Jyothi Karri
has been approved for the Department of Electrical Computer and Energy Engineering

Alan R. Mickelson

Dr. Won Park

Dr. Garret Moddel

Date

The final copy of this thesis has been examined by the signatories, and we find that both the content and the form meet acceptable presentation standards of scholarly work in the above mentioned discipline.

Karri, Jyothi (M.S., Electrical, Computer and Energy Engineering)

Tunable Multilayer Plasmonic Materials: Optical and Topographic Characterizations

Thesis directed by Dr. Alan R. Mickelson

The distinct behavior of structures of noble metals with nano-dimensions from that of the bulk metal in visible electromagnetic spectrum has provided access to exquisite characteristics and applications in the field of plasmonics. Plasmonics is a field of study of the interfaces of such metals and dielectrics. Embedding nanoparticles of noble metals in dielectric materials to achieve and tune plasmonic features to regions of spectrum, where naturally available materials do not exhibit such phenomenon, has been a subject of great attention for researchers.

In this thesis, I present the design and fabrication of coatings composed of thin metal and dielectric layers as a solution to tune the plasmonic features to other visible wavelengths and to near infrared regions and vary the optical properties of the coatings. Pushing down the limits on thickness of the layers far below the subwavelength dimensions has become a necessity to able to tune the plasmonic properties into the near infrared spectrum and beyond. This necessity has forced us to closely study the effects of roughness and continuity of the layers. These effects of pushing the layers to thinner dimensions on the optical properties will be presented and discussed with the aid of topographical nanoscopy images. Theoretical computations of transmission spectra of these coatings are accomplished using Maxwell Garnett approximation and a comparison with empirical results is presented.

First thin film flat layers are demonstrated to show the passive tuning of dielectric function, while supporting them with experimental results and theoretical simulations. In later part, thickness of the metal layers is decreased to limits where the effects of roughness and continuity of layers play a substantial role. The surfaces of layers are characterized in detail. A new efficient statistical model is developed that is built on the distribution of size and shapes of particles involved in percolation. This model is used to study the tuning abilities of these layers.

Dedication

To my Parents and my Husband.

Acknowledgements

In my pursuit of Masters, many a people have played a role or more (from lending AFM tips on time to addressing those haunting technical questions). The list would extend really long. I would like to express my gratitude to all of them and mention some of them here.

First and foremost, I am grateful to my advisor, Dr. Alan Mickelson for providing me the oppurtunity to work in his team, providing the ideas, the lab facilities and guiding me in the right direction. I really admire and am inspired by his quintessential skill of coming up with simple solutions to problems. I am grateful to ONR for funding my graduate study and again I thank Dr. Mickelson for choosing me.

I am obliged to my husband, Suresh Kumar Gollu for supporting me in all possible ways, motivating me and bearing with me. Suresh, continue the good work. My Parents, Ramu Naidu Karri and Nagamani Karri have always been very encouraging. I am forever indebted to them for believing in and supporting me. It is as much a triumph for them as for me.

I would like to thank Dr. Won Park for providing me with technical advices and discussions. I would like to thank all my course professors for teaching me the basics and nuances in the optics field which helped me in advancing my knowledge and applying it in my research work.

I would like to thank Dr. Xue Jiuzhi for valuable discussions, teaching me lot of fabrication processes and introducing me to cleanroom. I would like to thank my teammates Jian Wang, Brian Schwartz, David Espinoza, Jin Hyoung Lee and Xi Chen for timely helps and being such great friends.

Last and one of the most important, cheers to researchers (a few of them listed in references section) all over the world who shared their knowledge and results with us, which put us in a better position to be able to solve our problems.

Contents

Chapter

List of Tables

Table

List of Figures

Figure

Chapter 1

Introduction

In recent years, a huge deal of work is being put into developing materials that have negative dielectric function with very low absorption. Plasmonics is a field in which metal dielectric interfaces are studied [1, 2, 3, 4]. Low loss is a very significant factor that needs to be conquered to be able to use these materials in any application. Until couple of years, this absorption has been a very critical issue and would completely dominate any plasmon features. If the loss of plasmonic structures at visible wavelength scales can be kept under control through judicial design, a new generation of ultra thin optical components will result. Such promise has generated considerable interest in development and applications of plasmonic materials. Most of this thesis is focused on designing, simulating and fabricating materials with plasmonic properties in optical and near infrared spectrum and have low absorption. These materials are not naturally available. They are in general fabricated by embedding metal nanoparticles with different sizes, shapes and concentration in a range of dielectric materials by capitalizing on the phenomenon that a wave sees a heterogeneous medium as homogeneous medium if the elements causing the heterogeneity are smaller than the wavelength of electromagnetic wave. Changing the shape or fraction of the metal nanoparticles results in a change in the positions of resonances in the electromagnetic spectrum. This development is exploited to tune the plasmon wavelength in visible and near-IR (and in near future to mid IR too) regions of electromagnetic spectrum. These mixtures can be modeled through constitutive equations while conceding the averages of statistical variations of the elements in the material.

The main emphasis of this work is to demonstrate the sucsess of multilayered coatings for

achieving precise tuning of plasmonic behavior. In this process, it was very important to study the surface morphology of the layers of metals and dielectrics. This criticality of surface morphology is because the optical properties derive significant characteristics from the structure of layers. I show how these fabrication limitations result in bahaviour favourable in more than one direction of applications. Being able to simulate the consequences of surface irregularities on the scattering is advantageous for the design of any layer based devices (like surface plasmon polariton waveguides) and materials.

The outline of the thesis is as follows. In this chapter, I start with the definitions and relationships between optical properties of the materials and electromagnetic fields. In Chapter 2, I review the effective medium approximation technique used as applied to disordered metal structures of different shapes embedded in dielectric materials and the shortcomings of the methods, while supporting them with simulations. Chapter 3 presents characterization of surfaces of thin layers as the thickness of the deposited metal decreases establishing a theoretical model to relate optical properties with topology of surface. In Chapter 4, I compare theoretical and experimental results for thick and thin layers.

1.1 Electromagnetic Field and Optical Constants

When an Electromagnetic wave is applied to a dielectric material, the electron cloud and the nucleus in an atom act like a dipole and the dipole oscillates along with the wave, resulting in a dipole moment. The forces exerted by the field produce a polarization,

$$\mathbf{P} = \epsilon_0 \hat{\chi} \mathbf{E} \tag{1.1}$$

Where, $\boldsymbol{P}$ is the polarization vector and $\boldsymbol{E}$ is the applied electric field vector. $\hat{\boldsymbol{\chi}}$ is susceptibility tensor. For an isotropic material it would be a scalar. ϵ_0 is the free space or vacuum permittivity and is $8.852 * 10^{-12}$ F/m.

Electric displacement $\mathbf{D}$ is related to $\mathbf{E}$ by

$$\mathbf{D} = \epsilon_0 \mathbf{E} + \mathbf{P} \tag{1.2}$$

$$\mathbf{D} = \epsilon_0 \hat{\epsilon}_r \mathbf{E} \tag{1.3}$$

$\hat{\epsilon}_r$ is the relative permittivity tensor or dielectric function and $\hat{\epsilon}_r = 1 + \hat{\chi}$.

Similarly, the response to a magnetic field $\mathbf{B}$ can be defined in terms of magnetization $\mathbf{M}$ and relative permeability tensor $\hat{\mu}_r$.

$$\mathbf{B} = \mathbf{M} + \mathbf{H} \tag{1.4}$$

$$\mathbf{B} = \mu_\mathbf{0} \hat{\mu}_\mathbf{r} \mathbf{H} \tag{1.5}$$

$$\hat{\mu}_r = 1 + \hat{\chi_m}$$

$\hat{\chi}_m$ is the magnetic susceptibility and free space permeability $\mu_0 = 4\pi * 10^{-7}$H/m.

The combined effect of electric and magnetic fields in an isotropic material are described by Maxwell's equation, given below

$$\nabla \times \mathbf{B} = \mathbf{J} + \frac{d\mathbf{D}}{dt} \tag{1.6}$$

$$\nabla \times \mathbf{E} = -\frac{d\mathbf{B}}{dt} \tag{1.7}$$

$$\nabla . \mathbf{E} = \frac{\rho}{\epsilon_0} \tag{1.8}$$

$$\nabla . \mathbf{B} = 0 \tag{1.9}$$

In absence of free sources and charges, Maxwells equations reduce to

$$\nabla X \, \mathbf{B} = \frac{d\mathbf{D}}{dt} \tag{1.10}$$

$$\nabla X \, \mathbf{E} = -\frac{d\mathbf{B}}{dt} \tag{1.11}$$

$$\nabla . \mathbf{E} = 0 \tag{1.12}$$

$$\nabla . \mathbf{B} = 0 \tag{1.13}$$

Wave Equation given below in Eq.1.14 is a solution to Eq. 1.10 -1.13.

$$\frac{d^2\mathbf{E}}{dx^2} = \frac{1}{\mu_0 \mu_r \epsilon_0 \epsilon_r} \frac{d^2\mathbf{E}}{dt^2} \tag{1.14}$$

The multiplication constant on right hand side is the phase velocity, $v^2 = \frac{1}{\mu_0 \mu_r \epsilon_0 \epsilon_r}$ and the speed of light in free space is given as $c = \frac{1}{\sqrt{\mu_0 \epsilon_0}} = 3 * 10^8$ m/s. Thus, $v = \frac{1}{\sqrt{\mu_r \epsilon_r}} c = \frac{c}{n}$. Where, $n = \sqrt{\mu_r \epsilon_r}$ is the refractive index of the material. At optical frequencies, $\mu_r = 1$, concluding

$$n = \sqrt{\epsilon_r} \tag{1.15}$$

Refractive index is a measure of the behavior of the wave in a given medium whereas, relative dielectric function is a measure of the behavior of the medium when illuminated by an electric field.

Refractive index can be purely real or complex based on the type of material. For absorptive materials like metals, doped semiconductors that contain free charges, refractive index is complex and is denoted as,

$$\tilde{n} = n + ik \tag{1.16}$$

The real part, n gives the direction of the wave when it travels from one medium to other (Fig. 1.1)and the relation is given by Snell's law,

$$n_1 sin\theta_1 = n_2 sin\theta_2 \tag{1.17}$$

where n_1 and n_2 are the real parts of refractive indices and θ_1 and θ_2 are the angles made by the wave with the normal to the interface in the incident and exiting media respectively.

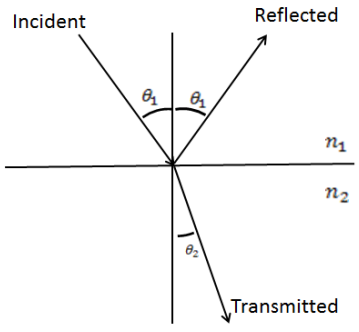

Figure 1.1: Snell's law gives the direction of transmitted wave in a medium on which a plane wave is incident. The direction of wave in second medium is dependent on the refractive indices on incident and refractive media and the angle of incidence in first medium.

Imaginary part k is called the extinction coefficient, a measure of the losses like absorption and scattering in the materials. It is related to absorption coefficient by,

$$\alpha = \frac{4\pi k}{\lambda} \tag{1.18}$$

$\tilde{n}$ as a whole is responsible for the direction and fraction of wave that are transmitted, reflected and absorbed. In a similar way, dielectric function is also a complex number for conducting materials. Dielectric function of metal is a key factor for the design and optimization of plasmonic nanostructures. It is a quantization of behavior of a material on application of an electric field. The resistance offered by a medium to an electric field is quantified by $\hat{\epsilon_r}$. It is a complex tensor for anisotropic lossy medium and reduces to a complex scalar ϵ_r for isotropic lossy medium. It varies with frequency for most materials, which is why materials behave differently to different kind of illumination. This frequency dependence reflects the fact that a material's polarization does not respond instantaneously to an applied field. The response must always be causal which can be represented by a phase difference.

$$\tilde{\epsilon_r} = \epsilon^{'} + i\epsilon^{''}$$

From Eq 1.15 and 1.16, the relation between refractive index and dielectric function concludes in

$$\epsilon^{'} = n^2 - k^2$$

$$\epsilon^{''} = 2nk \tag{1.19}$$

$$n = \frac{1}{\sqrt{2}}\sqrt{\epsilon^{'} + \sqrt{\epsilon^{'2} + \epsilon^{''2}}} \tag{1.20}$$

$$k = \frac{1}{\sqrt{2}}\sqrt{-\epsilon^{'} + \sqrt{\epsilon^{'2} + \epsilon^{''2}}} \tag{1.21}$$

$\epsilon^{'}$ is related to stored energy in the medium. $\epsilon^{''}$ is related to dissipation of energy in the medium, and is negative for a gain medium and positive for lossy medium. $\tilde{\epsilon_r}$ and $\tilde{n_r}$ satisfy Kramers-Kronig relation between their real and imaginary parts, which will be discussed in one of the subsequent sections.

1.2 Properties and Applications of Plasmonic Materials

Plasma is a gas of ions and electrons. Metals and doped semiconductors are composed of equal quantities of ions and mobile conduction electrons and they behave like plasma. Plasmonics is a field in which the metal-dielectric boundaries are studied. Plasmonic materials exploit the charges accumulated at metal-dielectric interfaces on application of an electric field i.e. surfaces plasmons. The free charges in metals do not experience any restoring force when an electromagnetic field is applied. Plasma frequency ω_p is the frequency at which the real part of dielectric function of the material goes to zero. For noble metals like silver, gold, copper etc., ω_p is in the visible regions of the spectrum. For $\omega > \omega_p$, $\epsilon^{'}$ is positive and for $\omega < \omega_p$, $\epsilon^{'}$ is negative. This negativity of the epsilon and position of ω_p are the reasons for the reflective appearance (Fig. 1.3) and the distinct colors of noble metals in visible spectrum. When $\epsilon^{'}$ goes to zero, $\epsilon^{''}$, which is proportional to absorption coefficient, dominates. At ω_p, oscillations of plasma take place. These oscillations are longitudinal, that is the electric field is in the same direction as the wave direction. This happens whenever $\epsilon^{'}$ goes to zero. The material is said to be plasmonic when the $|\epsilon'| > \epsilon''$. This behavior starts beyond plasma wavelength and lasts till collision frequency corresponding to collision wavelength,λ_c (listed in Table1.1).

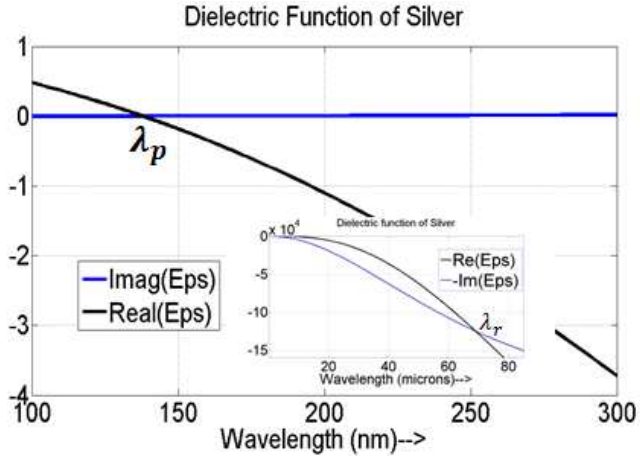

Figure 1.2: The wavelength at which real part of dielectric function crosses zero is called plasma frequency. Beyond this wavelength ϵ' is negative and till collision wavelength,λ_r $|\epsilon'| > \epsilon''$. Between λ_p and λ_r metals are plasmonic.

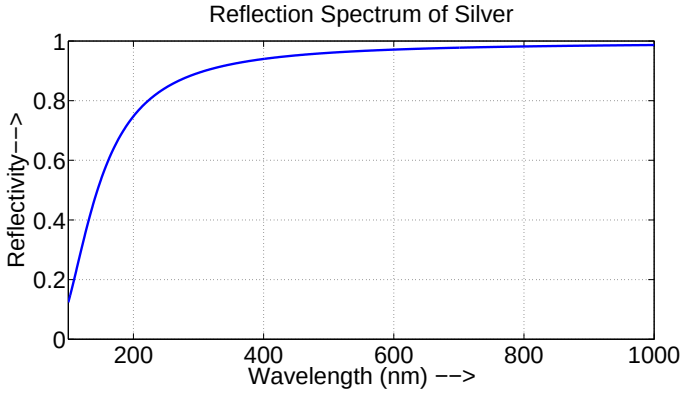

Figure 1.3: This picture depicts reflection of silver. This is an example of reflection of metals tending to unity beyond plasma wavelength ($138\,nm$) till the collision wavelength ($69\,\mu m$).

Low values for $\epsilon^{''}$ where $\epsilon^{'} = 0$ result in condition called epsilon near zero (ENZ). These materials are naturally available at limited wavelengths. So a combination of materials are used to achieve this phenomenon at wavelengths other than that are naturally available. This phenomenon

has been theoretically and experimentally tested for a number of applications[5, 6]. One of the applications is termed supercoupling [7], where a wave is guided successfully through narrow waveguides with arbitrary shapes which would have been very lossy if filled with a dielectric. The shift of plasmon absorption peaks are used to detect different types of molecules and proteins like Casein in milk [8], for transmitting data in processor chips [9], for plasmon based electronics like transistors, photodetectors [10]. Plasmons have also been successfully tested in lab for high resolution lithography and microscopy [11]. Embedding materials with magnetic resonances [12] into the ENZ materials results in zero index materials (ZIM), also known as metamaterials or left hand materials [13, 14]. The term left handed materials comes from the phenomenon that the light is refracted in the opposite direction than the usual right handed materials. In addition to being the most popular solution for the problem of reducing scattering from an object also called as cloaking [15, 16, 17, 18] and for achieving transparency [19], ZIM materials have found applications in near field superlens [20, 21, 22], in shaping the phase front of radiation [23, 24, 25]and directive emission [26].

1.3 Models for Dielectric Function of the Silver

The optical properties of metal particles are exceptionally different from that of bulk metal. Silver is studied in detail in this section owing to it's unique properties at visible frequencies. Silver particles that are small compared to the operating wavelength have very different behavior ftrom silver [27, 28, 29, 30]. The dielectric function of silver is dispersive i.e. it has different values as wavelengths varies. Silver has the lowest losses in the visible range Fig.1.5. Nanoparticles of silver exhibit plasmonic behavior. Different sets of dielectric function values and models for silver are available in literature. Some of them derived from experiments and others are based on oscillator models. As part of this behavior, the colors in stained glasses due to gold particles embedded in it was first investigated by Maxwell Garnett in 1904 and scattering from small particles was examined by Gustav Mie in 1908 [31] . Unlike dielectrics, metals like silver, gold, copper, etc. have dispersive optical properties, that is, the optical properties are highly dependent on wavelength. Optical properties of metals have been explicitly modeled. Two most extensively used models are

discussed below.

1.3.1 Drude Model

Drude model [32, 33]is the most used classical model for metals which has fairly good agreement with experimental deductions of dielectric functions in most of visible and near IR regions. Near the plasmon frequencies, it is not very accurate. For instance, the plasmon wavelength for gold is at 410 nm but Drude model predicts it to be at 138 nm, similarly for silver the plasmon wavelength prediction of Drude model is at 138 nm but experiments show it to be at 320 nm. This contradiction from Drude model to experimental results is due to the transitions from filled d band to sp conduction band.

The ionized atom and the free electron cloud in metals act like a dipole oscillator on application of an electromagnetic field. This behavior allows one to apply the Lorentz-Drude model to describe the optical properties of metals. The displacement of the atomic dipole is modeled as damped harmonic oscillators. The nucleus is far heavier than the electrons, so the motion of nucleus is ignored. The equation of motion of electron when an electric field $\mathcal{E}$ is applied is given as,

$$m_0 \frac{d^2x}{dt^2} + m_0\gamma \frac{dx}{dt} + m_0\omega_0^2 x = -e\mathcal{E} \tag{1.22}$$

where x, m_0, γ, e, and ω_0, are the displacement, mass, damping rate, charge and resonance frequency of the electron, respectively. Damping accounts for the collision of electrons with electrons, phonons, and lattice defects or grains boundaries. The terms on the left hand side are the acceleration, damping and restoring force, respectively. Since the restoring force on free charges is zero, the third term vanishes. Considering a monochromatic light applied, $\mathcal{E}(t) = \mathcal{E}_0 e^{-i\omega t}$, we would have solutions for displacement of the form $X(t) = X_0 e^{-i\omega t}$, which gives us

$$X_0 = \frac{e\mathcal{E}_0/m_0}{\omega^2 + i\gamma\omega}$$

The dipole moment due to the atomic dipole is $p(t) = ex$, which results in a macroscopic

polarization for N number of atoms per unit volume, $\mathbf{P}_{resonance} = Np = -Nex$.

$$\mathbf{P}_{resonance} = -\frac{Ne^2\boldsymbol{E}}{m_0(\omega^2 + i\gamma\omega)}$$

Due to this polarization term, Eq. 1.2 is modified to $\mathbf{D} = \epsilon_0\mathbf{E} + \mathbf{P}_{resonance}$ while $\mathbf{D} = \epsilon_0\epsilon_r\boldsymbol{\mathcal{E}}$ still holds good. Thus the expression for relative dielectric function tensor

$$\hat{\epsilon}_r(\omega) = 1 - \frac{Ne^2}{\epsilon_0 m_0(\omega^2 + i\gamma\omega)}$$

and we can define plasma frequency using this equation as

$$\omega_p^2 = \frac{Ne^2}{\epsilon_0 m_0} \tag{1.23}$$

$$\hat{\epsilon}_r(\omega) = 1 - \frac{\omega_p^2}{(\omega^2 + i\gamma\omega)} \tag{1.24}$$

ω_p is the plasma frequency. $\epsilon' = 0$. γ is the factor that causes damping and broadening of resonance. This value corresponds to collision frequency. The values for parameters of Drude model for some metals are enlisted in Table 1.1.

Drude model correctly predicts the qualitative shape of ϵ, and therefore produce fits with a relatively high degree of accuracy with a small number of free parameters. This model also obeys the Kramers-Kronig relations which constrain the relationship between ϵ' and ϵ''. But discrepancies have been found in values of ω_p from values that were measured, as explained in the next section, otherwise the values at non-resonant frequencies agree well with experimental results. This is because interband transitions are not considered in Drude model.

Table 1.1: The parameters for Drude Model of some metals.

Metal	Plasmon Wavelength (λ_p) in μm	Damping factor (γ) in μm
Silver (Ag)	0.138	69
Gold (Au)	0.13738	46.442
Aluminum(Al)	0.08406	15.15
Copper(Cu)	0.1677943	136.64
Platinum(Pt)	0.2410107	17.9

1.3.2 Kramers-Kronig Relation

Kramers-Kronig relation is a property connecting the real and imaginary parts of an analytic function. Because refractive index and permittivity are causal functions we can apply Kramers-Kronig relationship to calculate n from k and vice-versa and in the same way ϵ' from ϵ'' and vice-versa [34].

$$n(\omega) = 1 + \frac{1}{\pi} P \int_{-\infty}^{\infty} \frac{k(\omega')}{\omega' - \omega} d\omega'$$

$$k(\omega) = -\frac{1}{\pi} P \int_{-\infty}^{\infty} \frac{n(\omega') - 1}{\omega' - \omega} d\omega'$$

where P is the Cauchy principal value. A similar relation can be obtained for permittivity by replacing n by ϵ' and k by ϵ''. This is a very useful relation when inverting the optical properties from measured transmission and reflection spectra.

1.3.3 Johnson and Christy ϵ Values for noble metals

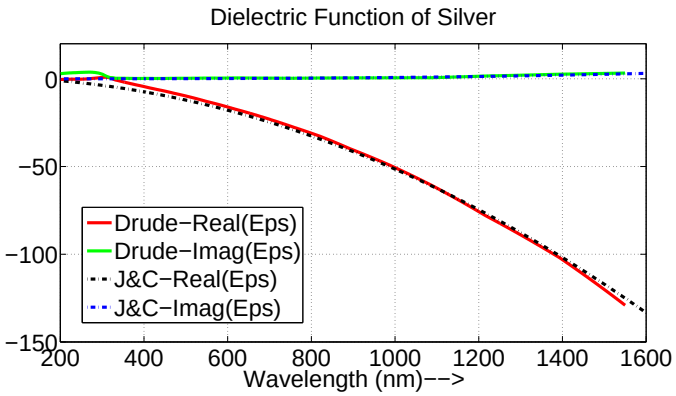

Figure 1.4: A comparison of ϵ of silver as a function of wavelength given by Drude model and Johnson and Christy. Clearly expect around $\lambda_p$these values overlap well but the prediction of λ_p by Drude model ($138\,nm$) is way off from experimentally determined J&C values ($310\,nm$).

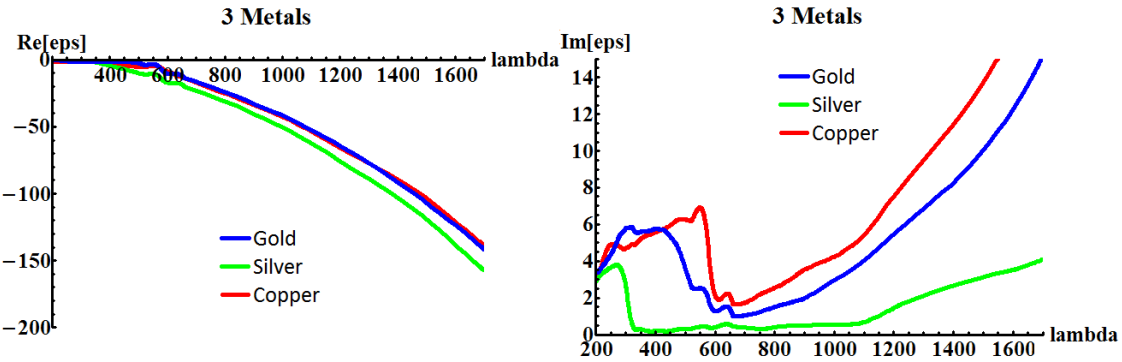

Figure 1.5: Comparing dielectric function of copper, gold and silver which exhibit plasmonic nature as a function of wavelength. For a wide range of wavelengths, the imaginary part of dielectric function is very low compared to other metals while the real part is almost identical.

In 1972, Johnson and Christy published their results for ϵ for silver, gold and copper inverted from experimental results [35]. Transmission and reflection spectra were measured at three different angles. ϵ were derived from these values. These values are found to be accurate to a reasonable degree when compared to results from more recent listings like [36, 37], though, there are still conflicts between these values, more so in the imaginary parts. The reasons for the conflict could be the surface roughness, resistivity of the layer and the substrate. These reasons will be studied further in chapter 3. Even more recent studies on silver have confirmed better accuracy of Johnson and Christy values [38]. The values of plasma wavelength has also been found to be in agreement with several publications. I used values from Johnson and Christy in wavelength range of 300 nm to 1900 nm, in this work. Fig. 1.5 plots the dielectric function of silver, gold and copper derived by Johnson and Christy. As we see the real part of ϵ of the three metals have almost the same behaviour in visible and infrared regimes. But silver has imaginary part that is much smaller than other metals. These low values for ϵ'' result in lower attentuation making silver suitable for many applications in plasmonics field.

Chapter 2

Effective Medium Approximation

2.1 Introduction

Composites of nano-particulates of plasmonic metals and dielectric hosts are widely used to artificially develop metamaterials. When dimensions of the inclusions are in subwavelength range, the inhomogeneous medium acts like a homogeneous and anisotropic medium. Effective medium theory describes the macroscopic properties of the mixtures based on the properties of the host and inclusions' properties and their relative fractions. To predict the effective optical properties of these composites there are classical mixing rules like Maxwell Garnett (MG), Lord Rayleigh and Bruggeman (BG) approximations available [39, 40, 41, 42, 43, 44]. Depending on the concentration and shape of the nanoparticles, these approximations result in effective permittivity. Though, there are other mixing methods available, involvement of a negative permittivity material rules their choice out due to surface plasmons [45]. Most of these theories fail to characterize the behavior close to a threshold value of the filling fraction where the inclusions are not isolated but are in contact in a critical fashion. In this chapter, I discuss BG and MG methods, their threshold values and their limitations. I will establish shape effects of nano-structures, shperoids in particular and present finite element method simulations for the resonance features for more random particles.

2.2 Bruggeman Approximation

Derivation of Bruggeman approximation starts by introducing voids of identical shape and size in a uniform medium. The change in conductivity due to these defects are summed. A different

kind of material is introduced into these voids. The polarization inside this void produces a change in field E_0 at the far field. An exact field around the particle is solved for and condition that the change in field is averaged out by the polarizations from the the two materials. This self-consistent requirement is solved for, to find the effective medium properties. Thus if we consider a host dielectric medium with dielectric function ϵ_d (that is constant over visible and near infrared wavelengths) and let there be identical metal nano particle inclusions of permittivity ϵ_m which are a fraction ϕ of the total volume and are oriented in same the direction. Bruggeman approximation for this biphase case gives the relation for ϵ_{eff} [46] of the composite as

$$\phi \frac{\epsilon_m - \epsilon_{eff}}{L\epsilon_m + (1-L)\epsilon_{eff}} + (1-\phi)\frac{\epsilon_d - \epsilon_{eff}}{L\epsilon_d + (1-L)\epsilon_{eff}} = 0 \tag{2.1}$$

For mixtures involving more than two components with same shape but different fill fractions,

$$\sum \phi_i \frac{\epsilon_i - \epsilon_{eff}}{L\epsilon_i + (1-L)\epsilon_{eff}} = 0$$

Where L is the depolarization factor of the inclusions which will be discussed in detail in the forthcoming sections. For spherical inclusions ($L = 1/3$), BG approximation is,

$$\phi \frac{\epsilon_m - \epsilon_{eff}}{\epsilon_m + 2\epsilon_{eff}} + (1-\phi)\frac{\epsilon_d - \epsilon_{eff}}{\epsilon_d + 2\epsilon_{eff}} = 0 \tag{2.2}$$

These comparisons of BG approximations [47] with numerical simulations using finite element method (FEM) indicate that BG is a good method to use in the high inclusion fraction limit, that is $\phi \to 1$. The region where it gives nearly accurate results is $\phi > 0.5$ in which the inclusions are not separated but are in contact with each other. Maxwell Garnett model, discussed in next section has been found to be more accurate in low metal fraction cases.

2.3 Maxwell Garnett Approximation

J. C. Maxwell Garnett was the one of the first researchers to study effects of inclusion in a host medium in a quest to understand the red color of ruby caused by spherical gold particles (that are small compared to the wavelength) and propose a model for effective permittivity [48, 49].

MG Approximation is the most widely used effective medium approximation. Maxwell studied and derived a model for spherical inclusions in a host medium based on propagating waves.

$$\frac{\epsilon_{eff} - \epsilon_m}{\epsilon_{eff} + 2\epsilon_m} = \phi \frac{\epsilon_d - \epsilon_m}{\epsilon_d + 2\epsilon_m} \tag{2.3}$$

This model inherently addresses the effects of the fraction of metal volumes and the interaction between adjacent particles, as it is derived from Clausius-Mossotti [50] which was based on Lorentz-Lorentz equation [51], which included the polarization effects from neighboring particles too. The significant feature of this approximation is the resonance that is predicted as the denominator of right hand side goes to zero. ϵ' never goes negative after the resonance and in the resonance regions where ϵ' does go negative, ϵ'' has an absorption peak, making the plasmonic region almost non existant. This resonance is dependent on the fill fraction of metal inclusions. As the filling factor increases, the resonance shifts to red and gets broader (Fig. 2.1). From simulations shown in Fig. 2.1, it is clear that the spectral range over which this resonance can be tuned using clusters of nanospheres is limited, dismissing all the proposals to use them for tuning this resonance to near-IR regions. This again fails the usage of clusters of nano-spheres for plasmonic applications. Acheiving high fractions of metal nano spheres without agglomeration is a hard task. A maximum of only 70% only has been obtained in laboratories. Even if high filling factors were achieved without agglomerations, λ_p can be tuned only in a limited spectra. The solution I demonstrate with metal-dielectric thin films is much more efficient, practical and simpler process.

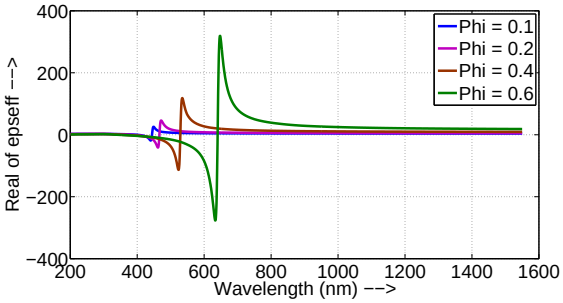

Figure 2.1: Resonances of clusters of nanosphere embedded in a host medium of $PI - 2555$. The fill fraction of spheres is varied to notice that the resonance shifts to red and gets broader.

The approximation Eq. 2.2 did not address for inclusiond that are spherically non-symmetric which we often come across in this study. An extension to the method proposed by Maxwell Garnett to non-spherical particle inclusions was published by Galeener in 1971[52], taking into consideration the depolarization factor L [53, 39], a shape dependent and size independent parameter [54]. But they assumed a spherical Lorentz cavity and were proved wrong by Cohen et al. [55]. Cohen et al. corrected the Lorentz cavity to be of the shape of the particle hence using same depolarization factor for calculating effective field as that appears in the response of ellipsoidal region to an applied field. This is apparent as the electric field at the point of observation is due to the lowering of field by the polarized volume. The following was the result,

$$\frac{\epsilon_{eff} - \epsilon_m}{L\,\epsilon_{eff} + (1-L)\,\epsilon_m} = \phi \frac{\epsilon_d - \epsilon_m}{L\,\epsilon_d + (1-L)\,\epsilon_m} \tag{2.4}$$

where ϕ is the fraction of metal inclusions, ϵ_d, ϵ_m are the permittivity of the metal inclusions and host dielectric, respectively. Depolarization factor L is discussed in detail in section 2.4. When $L = 1/3$, the case of spherical particles is obtained. This MG model is good only when all particles are of same shape, if there is a statistical distribution, MG does not hold good. In subsequent chapter, a novel method taking into account these distributions is presented. Cohen et al. [55] compared the results from the above dielectric theory and figured out that it's validity is limited to a threshold $\phi < 0.6$. This threshold value itself has been studied and varied results were published ranging from 0.5 to 0.7 [55, 56]. As long as the particles are separated MG is valid and this decides the threshold value. Thus even if high fill fractions were involved, as long as the particles are well separated MG is valid. To accomplish this nanoparticles of metals are coated with surfactants like Tween 20 for gold particles and SiO_2 for silver particles. Over this threshold value, the extended Maxwell Garnett theory ceases to agree with measurements. The effective dielectric function is given as,

$$\epsilon_{eff}(\lambda; L) = \epsilon_d(\lambda) \frac{(\epsilon_m(\lambda) - \epsilon_d(\lambda)\,(\phi + L(1-\phi)) + \epsilon_d(\lambda)}{L(\epsilon_m(\lambda) - \epsilon_d(\lambda))\,(1-\phi) + \epsilon_d(\lambda)} \tag{2.5}$$

All the dielectric functions are being represented as a function of λ to emphasize that effective permittivity depends on wavelength too. The resonance wavelength for the effective medium can be obtained by equating the denominator to zero, $L(\epsilon_m(\lambda) - \epsilon_d(\lambda)\,(1-\phi) + \epsilon_d(\lambda) = 0$. Hence, for a given host material embedded with metal inclusions, the value of ϵ at which we would see a resonance depends on the fraction of metal and shape of the particle.

$$\epsilon_m(\lambda) = \epsilon_d(\lambda)\frac{L(1-\phi)-1}{L(1-\phi)} \tag{2.6}$$

By considering ϵ_d to be constant over the spectrum of interest, if we map ϵ_m to Drude model, we can find an approximate resonance wavelength for the composite,

$$\lambda_{dr} = \left(\frac{(1+\phi\epsilon_d)\lambda_p^2\lambda_0^2}{\lambda_0^2 - (1+\phi\epsilon_d)\lambda_p^2}\right)^{1/2} \tag{2.7}$$

2.4 Depolarization Factor

Consider an ellipsoidal particle embedded in an electric field. Due to the small size of the particle, the induced dipole field that forms inside it on application of an external field is uniform. This induced field is due to the uniform polarization in the particle and it tends to oppose the applied field and thus this field is called depolarization field. This causes a depreciation of effective field outside the particle. Thus the effective field acting on the dipole is $\mathbf{E} + \hat{\mathbf{L}}\mathbf{P}/\epsilon_0$. It is a measure of the ratio of the induced electric field due to surface charges on the particle to the polarization of the material. It is a factor strongly dependent on the shape and orientation of the particle. In Cartesian coordinates, components of depolarization field, $\mathbf{P}$ can be represented as P_x, P_y and P_z along the principle axes of the ellipsoid and can be written as,

$$E_x = -L_x P_x/\epsilon_0 \qquad E_y = -L_y P_y/\epsilon_0 \qquad E_z = -L_z P_z/\epsilon_0$$

L_x, L_y and L_z are the depolarization factors [53] in the respective directions and satisfy $L_x + L_y + L_z = 1$ and $0 \leq L_{x,y,z} \leq 1$. For a random shaped particle or if the axes of the ellipsoid does not align with the coordinate axes, $\hat{L}$ is a more involved tensor.

For an ellipsoidal particle, L is dependent on the ratio of its major to minor axis. In this case, $L_{x,y,z}$ are the principle elements and are given by,

$$L_x = \frac{abc}{2} \int_0^\infty \frac{ds}{(s+a^2)R_s} \tag{2.8}$$

$$L_y = \frac{abc}{2} \int_0^\infty \frac{ds}{(s+b^2)R_s} \tag{2.9}$$

$$L_z = \frac{abc}{2} \int_0^\infty \frac{ds}{(s+c^2)R_s} \tag{2.10}$$

Where $s = \sqrt{(a^2+b^2+c^2)}$. From the above equations we can conclude that if $a > b > c$, we have $L_x < L_y < L_z$. So, depolarization factor is strongly dependent on the symmetry of the particle.

Oblate and prolate spheroids are most useful ellipsoids. For an oblate nanospheroid with semi axes (a, b, c) in (x, y, z) directions and $a = b,\ b > c$, the depolarization factors satisfy [53], $L_x = L_y = 1/2(1 - L_z)$. L_z in this case is a function of the eccentricity of the spheroid, $e = \sqrt{b^2/c^2 - 1}$ and is given as,

$$L_z = \frac{1+e^2}{e^3}\left[e - tan^{-1}e\right] \tag{2.11}$$

For a prolate nanospheroid with semi axes (a, b, c) in (x, y, z) directions and $a = b,\ c > b$, the depolarization factors satisfy [53], $L_z = (1 - 2\,L_x)$. L_x is a function of the eccentricity, $e = \sqrt{1 - b^2/a^2}$ and is given as,

$$\mathrm{L_x = L_y} = \frac{1-\mathrm{e}^2}{2\mathrm{e}^3}\left[\log\left(\frac{1+\mathrm{e}}{1-\mathrm{e}}\right) - 2\mathrm{e}\right] \tag{2.12}$$

When the ellipsoids are randomly oriented in the given mixture, the effective dielectric function is given by [57]

$$\epsilon_{eff}(\lambda) = \frac{1}{3}\sum_{i=x,y,z} \epsilon_{eff}(\lambda; L_i) \tag{2.13}$$

where $\epsilon_{eff}(\lambda; L)$ is given by Eq. 2.5 or Eq. 2.1.

L is related to structural electromagnetic resonance. Fig. 2.2 shows some simulations of these resonances and depolarization factors for oblate and prolate nanospheroids that are embedded in $PI - 2555$ host medium with a fill fraction of 0.5. Fig.2.2(a) displays how the depolarization factor

changes with the aspect ratio of the spheroid. Fig. 2.2(b) is a plot of resonances for different aspect ratios. In relation to these ratios, Fig. 2.2(c) displays the actual effective permittivity of the homogenized medium, for cases of spheres and oblate spheroids with different depolarization factors. We can see for a sphere there is one resonance and as we deviate from this spherical symmetry, the resonances split and shift to different wavelengths. These effective permittivities are used to plot transmission for a layer of this mixture, Fig. 2.2(d). Sphere due to its symmetry has $L_x = L_y = L_z = 1/3$ and hence has one resonance, it is illustrated in 2.2(c) for a silver particle, starting with a spherical shape. As the shape deviates from this spherical symmetry, the resonance splits up into more number of resonances in the electromagnetic spectrum. As the particle flattens from a spherical shape to an oblate spheroid, L_z increases (L_x and $L_y$decrease) until its value reaches maximum of 1 where the particle is a flat plate for which, $L_x = L_y = 0$ and $L_z = 1$. In terms of structural resonance this can be explained as follows. As the particle flattens from being a sphere (which has one resonance) to a more flat oblate, the resonance splits and each resonance moves in opposite directions. One resonance moves to lower wavelengths and another moves to higher wavelengths until it becomes a flat plate where the lower resonance moves to the material plasma wavelength and higher reaches the collision wavelength (listed in Table 1.1).

2.4.1 Finite Element Simulations for Resonances

Analytic determination of resonances and depolarization factors for spheroids has been detailed in previous section. But for particles of arbitrary shape, an analytical solution is very tedious. So best solution is to use numerical methods. In this section, I present one such finite element method to demonstrate the resonances of particles of various shapes. A quasistatic technique in line with the method described in [58], combined with finite element method is used to predict the resonance for particles of different shapes. A similar numerical technique to determine L for more complex, arbitrary shapes has been discussed in [59]. I used COMSOL Multiphysics to accomplish

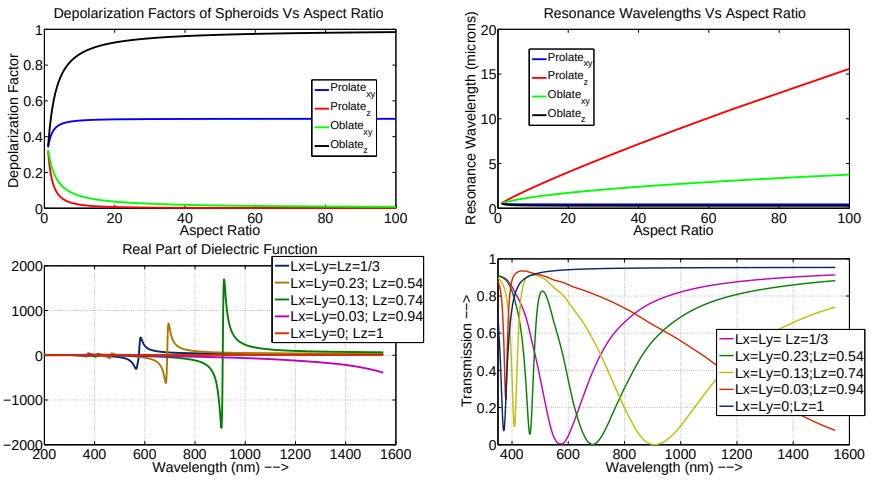

(d)

Figure 2.2: This figure is to demonstrate the change in optical properties of nanospheroid with changing aspect ratio. The particles are considered to be embedded in PI-2555 host medium. (a) shows the variation of depolarization factor in lateral and transverse directions with aspect ratio of the particle. (b) gives the resonance wavelengths for different aspect ratios. (c) shows the actual dielectric function with shifted resonances for sphere and oblate spheroids. Sphere has aspect ratio of 1 and has one resonance at 550 nm when fill fraction of metal is 0.5, as aspect ratio deviates from 1, the resonances due to transverse and lateral dimensions separate and shift in opposite directions.(d) is the transmission of a layer filled with particles shaped as sphere and oblate spheroids with different aspect ratios.

these simulations in 2D and 3D. Consider a particle with a dispersive dielectric function. A voltage potential is applied in $y-$direction. The particle has dimensions smaller than the wavelength, so that the electric field is uniform across the particle and also that the surface effects are substantial. For particles with bigger dimensions, the surface effects are relatively feeble. In this approach, the optical absorption is associated with polariton normal modes.

An electric field is applied in $y-$direction and periodic boundary conditions to the faces in $x-$ and $z-$ directions. The surface polarization modes are determined by scanning across the negative real permittivity, and the corresponding wavelength values are mapped out from the dispersion relation of the material. A particle with a given shape has a number of strong normal modes that depend on the symmetry of its shape and thus we would see as many absorption peaks. For instance sphere has one normal mode and a cube has six. To reinforce on our previous results, we see two resonances for spheroids that are deformed from spherical symmetry that are shifting in opposite

directions, as shown in Fig.2.3 and 2.4. To map the resonances to depolarization factor we use MG Eq.2.5. Depolarization factors thus calculated for a cube are tabulated in Table 2.1. Fig. 2.7 shows the normal modes in a cube. There are more absorption peaks but only six are significantly strong. As the symmetry of cube is disturbed, more and more resonances appear, some with small strength adn other with significantly higher strength. The same results are noticed when one of the dimensions of the cube is increased to make it a cuboid, as shown in Fig. 2.6.

Table 2.1: Depolarization factors and $\epsilon_m$values at which resonances for a cube occur are tabulated. These are the strongest resonances. Others are relatively weak.

Depolarization factor,L	ϵ_m
0.0649	-14.4
0.0746	-12.4
0.0877	-10.4
0.1042	-8.6
0.1163	-7.6
0.1471	-5.8
0.1724	-4.8
0.2174	-3.6

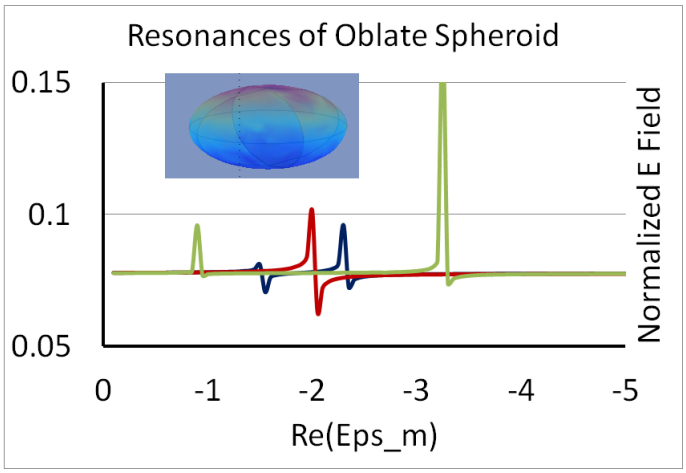

Figure 2.3: FEM simulation of resonance of a sphere and oblate spheroids. Sphere has one resonance at $\epsilon_m = -2\epsilon_d$ and $\epsilon_d = 1$ and oblate spheroid has two resonances shifted that move in opposite directions as aspect ratio increases.

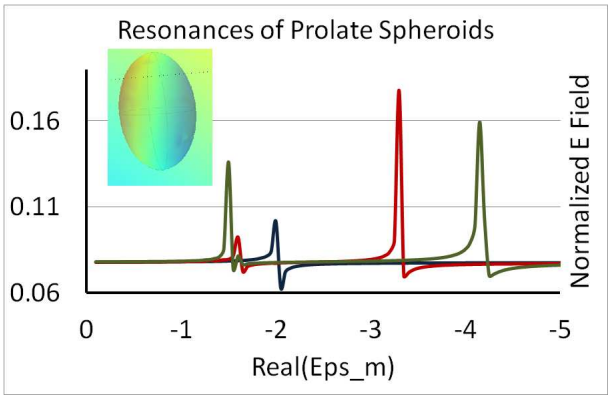

Figure 2.4: FEM simulation of resonance of a sphere and prolate spheroids. Prolate spheroid has two resonances shifted that move in opposite directions as aspect ratio increases.

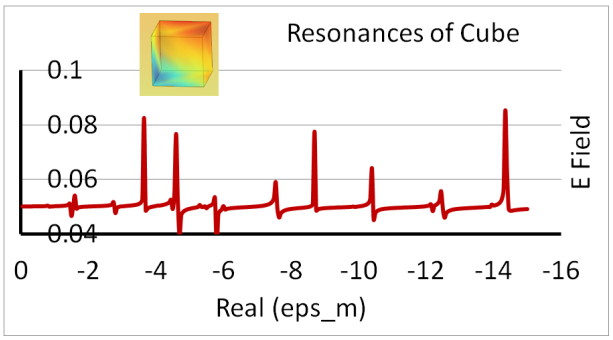

Figure 2.5: FEM simulation of resonance of a cube. Cube has six normal modes with significant strength and thus as many resonances.

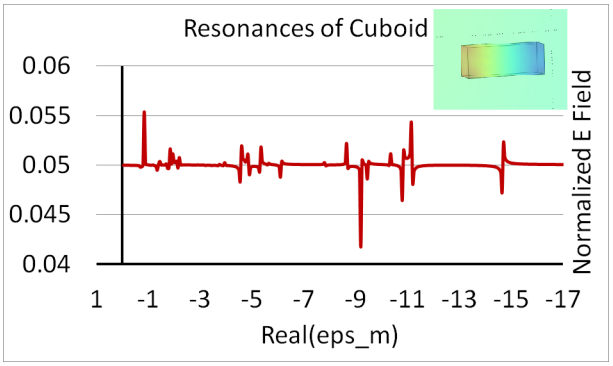

Figure 2.6: FEM simulation of resonance of a cuboid. Cuboid is a cube with one elongated dimension. So it has more number of normal modes thus resonances.

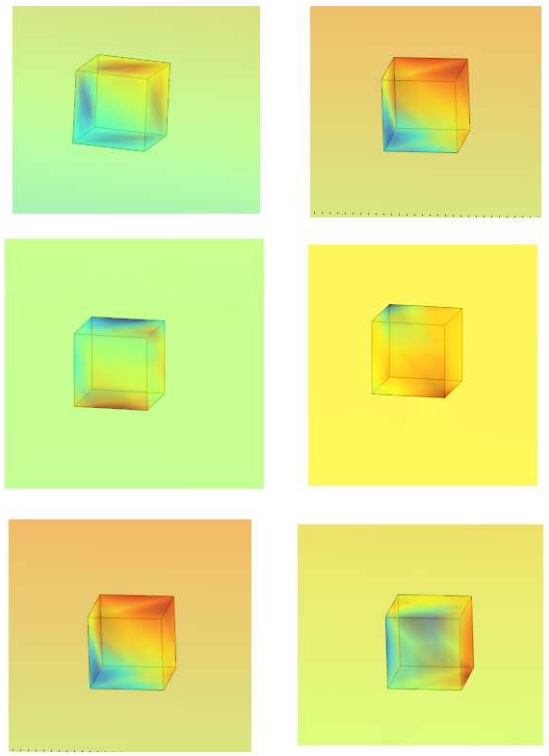

Figure 2.7: Cube has these dominant six normal modes.

2.5 MG for Thin Flat Layers

Maxwell Garnett emerges out to be a very advantageous tool for approximating the effective medium properties of thin flat layer stacks. When the thickness of layers is significantly smaller than $\lambda/4$, the inhomogeneous stack acts like a homogeneous medium that is highly anisotropic. As discussed in the earlier section, $L_z = 1$ for flat plates, that is when incident light is polarized parallel (TM polarization) [60] to the plane of layers. If the light is polarized perpendicular to the plane of layers (TE polarized), $L_z = 0$. In the former case, the stack of layers act like capacitors in parallel, and the effective permittivity is given as the weighted average of the permittivity values of the materials of layers in the stack. Hence, if there are two different materials involved, the effective

dielectric function is,

$$\epsilon_{eff}(\lambda; L = 1) \ = \phi_1 \, \epsilon_1(\lambda) + \phi_2 \, \epsilon_2(\lambda) \tag{2.14}$$

where $\phi_{1,2}$ are the volume fraction of materials of $\epsilon_{1,2}$, and $\phi_1 + \phi_2 = 1$. For thin flat layers, relative thickness is the measure of the $\phi_{1,2}$. We use this particular phenomenon to design and explain the layered structures with tunabe plasmonic features.

If the stack has layers of n kinds of materials, we can generalize Eq 2.14 and deduce

$$\epsilon_{eff}(\lambda; L = 1) \ = \sum_{k=1}^{n} \phi_k \, \epsilon_k(\lambda), \qquad \sum_{k=1}^{n} \phi_k \ = 1 \tag{2.15}$$

When the light is polarized perpendicularly to the surface of layers, the stack would act like capacitors in series and the effective permittivity is given as

$$\frac{1}{\epsilon_{eff}(\lambda; L = 0)} = \frac{\phi_1}{\epsilon_1(\lambda)} + \frac{\phi_2}{\epsilon_2(\lambda)}$$

Comparisons of several simulations, multilayer theory and effective medium theory have shown that certain conditions need to be satisfied for applying effective medium thoery to thin film stacks. The main conditions that need to be satisfied in order for effective medium approximations to be valid is that 1) the optical thickness of each layer is smaller than a quarter of the wavelength of operation,$\lambda/4$ and 2) the period thickness of the layers should also be smaller than $\lambda/4$. When these conditions are not met, then the layered structure is no more a homogeneous medium.

A comparison of transmission calculated using MG and Fresnel's multilayer theory is demonstrated in Fig. 2.8 for a stack of layers composed of silver and PI-2555 [9] (refractive index 1.7) layers. Fresnel's multilayer theory (A) is an accurate and well accepted method to predict transmission and reflection from thin flat layers. Fig. 2.8(a) shows a comparison of cases when both the conditions stated above are satisfied. The deviation of MG from multilayer theory is evident in Fig. 2.8(b). The plots with MG-120-5 indicate that the dielectric layer thickness is 120 nm and that of silver is 5 nm. Here optical thickness of PI-2555 layer exceeds λ thus condition 1 is not satisfied. In the case of MG-90-5 the period thickness is greater than the $\lambda/4$ and demonstrates the need to have the period thickness smaller than $\lambda/4$.

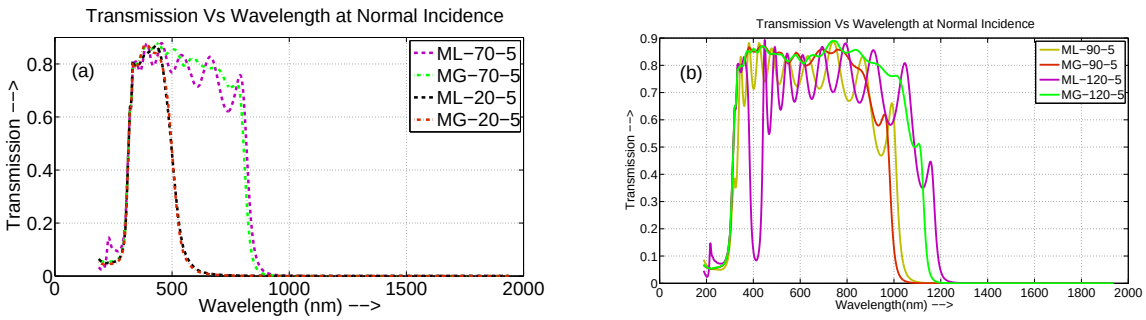

Figure 2.8: Comparison of MG and ML theory for stack of $PI - 2555$ and Ag layers: (a) shows cases where both layer thickness and period thickness are smaller than $\lambda/4$, hence multilayer theory matches well with transmission using MG theory. (b) These are the two cases when MG does not agree with ML theory. The MG-90-20 is the case where both the layer thicknesses are less than wavelength but the period thickness is higher than $\lambda/4$ and MG-120-5 is when layer thickness of $PI - 2555$ exceeds $\lambda/4$.

Chapter 3

Characterizations of Thin Films

In the previous chapters it was established that the thicknesses of layers are very critical formaking plasmonic coatings and that the metal layers need to be made very thin in order to satisfy the conditions for effective medium approximations. The study of surface quality of thin films becomes very critical when the thickness of films is very low. If the metal layer is relatively thick (>15 nm), the surface effects are less significant but as the thickness of layer decreases, surface effects are substantial. In case of thin metal films at low thicknesses, along with the surface effects, the imaginary part of dielectric function differs from ideal bulk metal [30, 38, 29]. Size effects become more significant as the dimensions become smaller than the electron mean free path, which is about 50 nm for silver [61]. Thin film stacks have a wide range of applications from high quality mirrors to plasmon polariton waveguides. The effectiveness of these stacks in these applications can be improved if the effects of roughness are comprehended. In this chapter, I will discuss the fabrication techniques used for all the samples used in the work and present some images from atomic force microscope (AFM) and scanning electron microsopce (SEM) for relatively thick and thin films of $PI-2555$ and silver. I derive a model based on statistical distribution and MG approximation showing the effects of roughness of metal layer is developed.

3.1 Fabrication of Thin Films

3.1.1 Silver Deposition

Silver was deposited by evaporation in a vacuum chamber. The evaporation rates between $0.03\,nm/s$-$0.1\,nm/s$ were used, depending on the end thickness. As shown in section 2.5, the thickness of the films need to be lesser than wavelength of operation, so we need to use thin layers for tuning plasma wavelength to infrared regions. But as we go to lower thicknesses the properties of silver layers are very different. The reasons are explained below.

Metal layer deposition by evaporation or sputtering is a dynamic process. The film growth by evaporative metal deposition consists of three stages. As time progresses the three stages occur. In the beginning (0-2 nm) , that is at very low thickness the layer would just be a collection of islands at this stage it is called a percolated layer. These islands have varied dimensions that are random about an average value. With time these islands grow bigger to agglomerate. This is the stage where the islands are touching each other but the layer is still incomplete with a roughness (2-15 nm). Then in third stage (>15 nm) these islands gradually homogenize to form a uniform layer [61]. The time and thickness scale of this process is dependent on a myriad of factors, like the vacuum level in the chamber and the temperature of the substrate [56]. We used a desktop evaporator from Balzers (with vacuum pump BZ 43 , Balzers PKG-020 gauge Control and evaporation unit BAE-080T). In our study, we grew metal layers with thicknesses from 2 nm to 20 nm. At a 2 nm thickness, the silver layer is fully percolated, that is, it consists of isolated particles of silver.

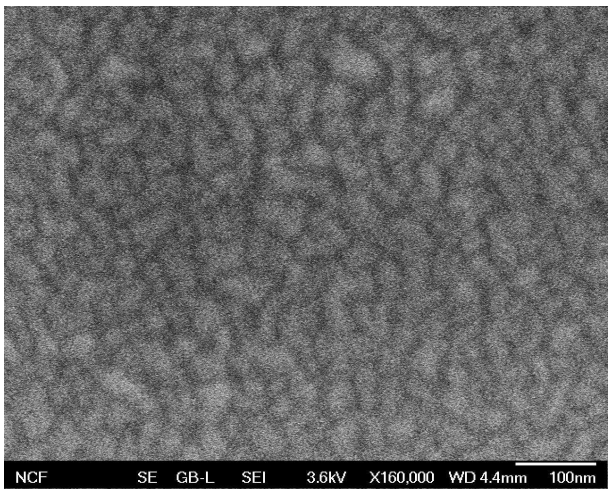

Figure 3.1: A scanning electron micrograph (SEM) image is a 4 nm Ag layer evaporated on glass substrate. Scale shows that the metal islands are of varied sizes and the islands are connected to form a semi-continuous layer. The transverse scale of the particle sizes are about $20 \pm 5\, nm$.

At a thickness of 4 nm, the layer appears as depicted in Fig. 3.1 and Fig. 3.2, that is, the layer is a group of connected islands of varying thickness. A series of AFM measurements are shown here to compare the surfaces of thin and thick layers of Silver. Fig. 3.2 shows surface of morphology 4 nm thick Ag layer at a scale of 100 nm.

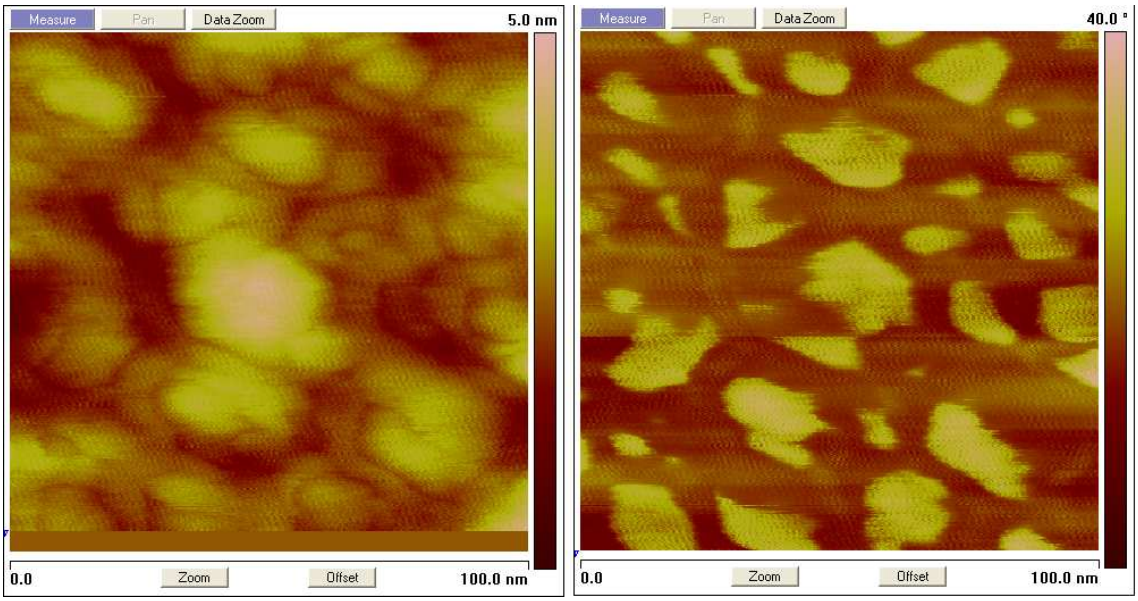

Figure 3.2: Surface morphology of a 4 nm Ag layer deposited on glass substrate measured using an atomic force microscope Veeco Dimension 3100 AFM). The image on left shows the height variation and the one on right shows the phase variation. The height scale defined left each pictures indicates that the roughness of the layer is about $3 \pm 1\,nm$ and diameter in the lateral dimension is about $20 \pm 5\,nm$.

The roughness on this layer is visible with an RMS of 3 nm with the lateral dimension of involved particles being 20 nm to 30 nm. An SEM image also shows the same particle size, Fig. 3.1. At such a thickness, the islands are connected, but still have a significant standard deviation in both height and transverse dimension. The 8 nm layer has many of the characteristics of the 4 nm layer. It is important to note that the crystalline quality of the silver is preserved in all the stages. The X-ray diffraction spectra given in [61] show that all the diffraction peaks are consistent.

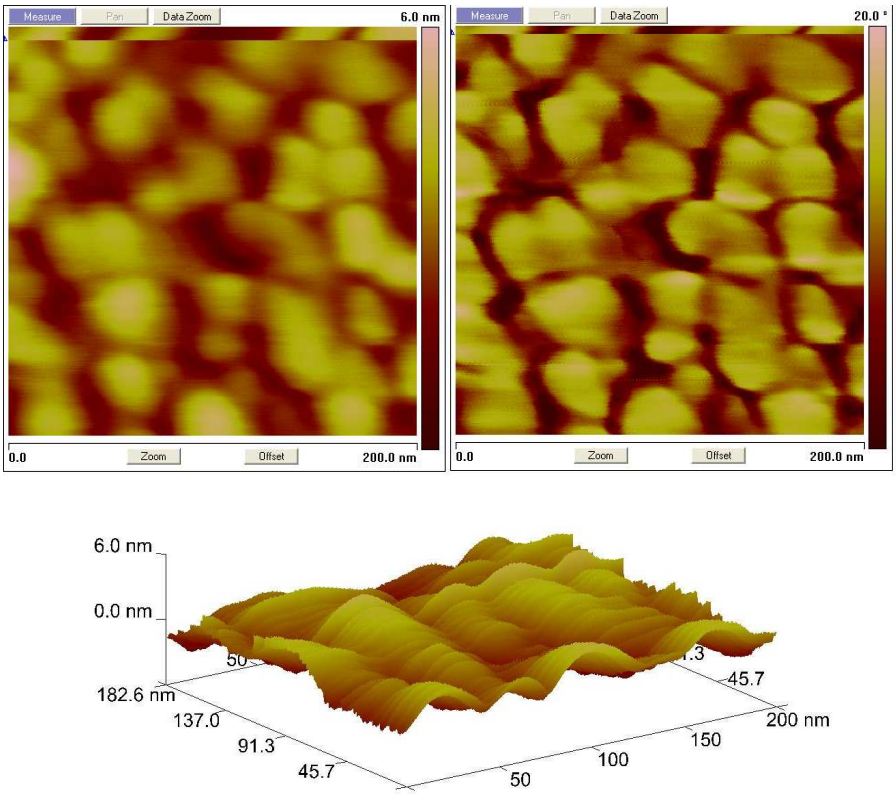

Figure 3.3: An AFM micrograph of a 20 nm Ag layer. This is on a scale of 200 nm. The layer is still rough with an RMS of the roughness is about 4 nm.

Fig. 3.3 shows surface of a 20 nm thick layer. The roughness on this one is about 4 nm. This is kind of roughness on a 20 nm layer layer does not have very significant effects on the overall optical properties the reason will be discussed in next section. There are numerous applications for such percolated layers if the morphology can be controlled and characterized well [62, 63]. The morphology of these layers can be controlled to some level [56] with the aid of physical parameters like temperature but not to a great extent. Some of the applications are discussed in [62].

3.1.2 Polymer Deposition

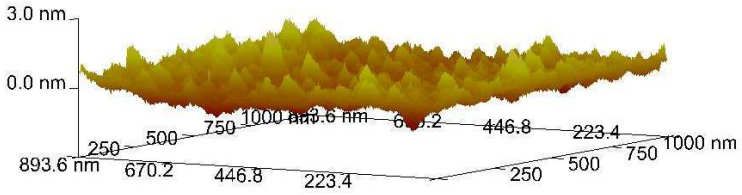

Figure 3.4: This shows a micrograph of PI-2555 layer that is 40 nm thick. The RMS roughness on this layer is less that 3 nm.

To accomplish the required design for tuning λ_p, we need to make stacks of silver and polymer layers. In order to have homogeneous material, we need to push the limit on thickness of polymer layer down too. Polyimide $PI-2555$ has an index of refraction of 1.7 over visible, near IR and most of mid infrared region. The high index helps in tuning $\lambda_p$to higher wavelengths. This PI has a low cure-temperature of 100^0C . Low temperature is very essential as it would reduce the delaminating of deposited silver layers caused by high temperatures. Polyimide has a very good thermal and environmental stability. Loss at visible wavelengths is $0.3\,db/cm$ [64]. Sodalime substrates were used for all the samples. The substrates are first cleaned using alconox and then the polyimide layers are spin-coated on them. To deposit thin layers $PI-2555$ diluted to about10%$-$30% by volume in $N-Methyl\ 2-pyrrolidone\,(NMP)\ solvent.$ In the first step, 20% $PI-2555$ was spun at speed of 300 rpm for 30 s which is an intermediate spin stage to allow the polyimide to spread evenly over 80% of the substrate. At a low acceleration of 100 rpm/s the final spin speeds of $3500\,rpm$, $3000\,rpm$ or $2500\,rpm$ is reached and is spun for $30s$ at these speeds. The final speed determines the thickness of the layer. It is then pre-baked at 90^0C for 15 min and cured at 100^0C for 45 min , which resulted in a 130 nm thick $PI-2555$ layer. During curing, the polyamic acid is converted to polyimide and the solvent is completely driven off. Table 3.1 shows a spin curve

determined for $PI-2555$, after measuring the deposited layers with Dektak. Fig. 3.4 shows surface morphology of a 40 nm PI-2555 layer. The roughness of layer is about 3 nm. This kind of roughness can be maintained with proper calibration of spin speeds and spin periods.

Table 3.1: Table listing the thicknesses of Samples with rough layers of silver layer that were fabricated and measured.

Sample Number	PI-2555 Thickness (in nm)	Ag Thickness (in nm)
Sample 1	40	4.1
Sample 2	50	7.1
Sample 3	76	8

3.2 Optical Properties of Thin Silver Layer

As we study silver layers with decreasing thickness, we notice that below a threshold value for thickness the permittivity values are different from one thickness to other. Over this threshold thickness, ϵ values stabilize and agree with [35] for highly pure and smooth silver layers. This is due to the particle nature of the thin layers and due to the shape distribution of those particles. The index of refraction,n increases with increasing thickness until a threshold thickness is reached but beyond that threshold, n stabilizes. Due to the discontinuity of the layer, electrons are trapped in the voids and surface plasmon resonances are induced. This causes an increase in the absorption. As the surface becomes smoother and continuous, the electrons are capable of moving freely and the probability of excitation of surface plasmons and amplitude of absorption decrease.

Transmission measurements from a 4 nm thick layer were made. Fig. 3.5 shows a comparison of measured transmission and transmission calculated using Johnson and Christy's values for a 4 nm flat layer and multilayer theory. The huge conflict between the two is due to the deposited layer being percolated (Fig. 3.2). The measured transmission flattens which is an indication of

formation of surface charges on the percolations. For a percolated layer, we cannot just use the Fresnels relations. To characterize these layers, the first step would be to model dielectri function of these layers. We need to use the MG approximations to model silver inclusions in air dielectric host. The following section describes in detail the method to deal with roughness effects on permittivity. Besides considering the roughness, the loss also increases because of the scattering by the particles. The surface scattering losses are in the order of $10^{-5} - 10^{-4}$.

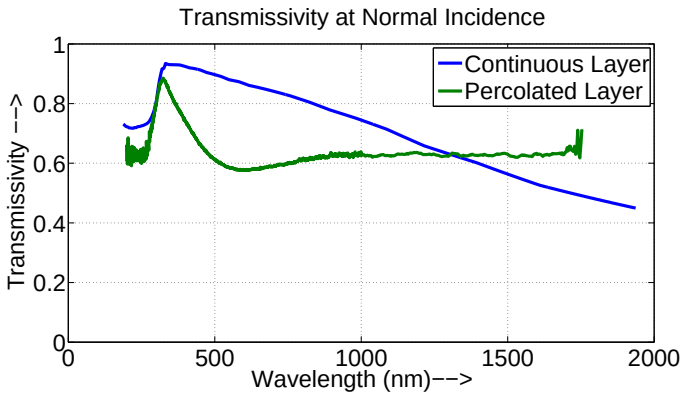

Figure 3.5: This a comparison of transmissivity measured from a percolated 4 nm Ag layer with transmittance calculated using J&C values and multilayer theory for a continuous smooth layer.

3.3 Modeling Rough and Percolated Layers

Fig. 3.5 proves that using multilayer theory alone with J&C values for ϵ does not suffice to characterize the thin metal layers that are percolated or rough. In this section, I present a method to model such layers. This is an efficient method for characterizing the permittivity of rough layers based on the distribution of shape of the particles.

3.3.1 Percolated Metal Layer

For very thin layers with thickness less than $2\,nm$, layers are isolated islands and a thicker layer has connected islands. When the islands are isolated, charges accumulate on the surfaces of the

metal particles and surface plasmons are induced resulting in a condition where the effective medium acts like a capacitors in series. Each particle will have a surface plasmon resonance corresponding to its shape or aspect ratio which is also affected by interaction with neighboring particles, which results in inhomogeneous broadening of the plasmon resonance [65]. The particles are of random sizes but can be approximated as oblate nanospheroids considering their symmetry in the xy-plane.

From the AFMs and SEMs (Fig. 3.2), we notice that the particles are in the size range of $20\,nm - 30\,nm$ in lateral direction. In transverse dimension, the particle size is between $2\,nm - 4\,nm$. The aspect ration of these particles corresponds to betweeb L of 0.05 and 0.2. Fig. 3.6 shows a distribution of particles of different depolarization factors in the AFM image measured on the silver layer.

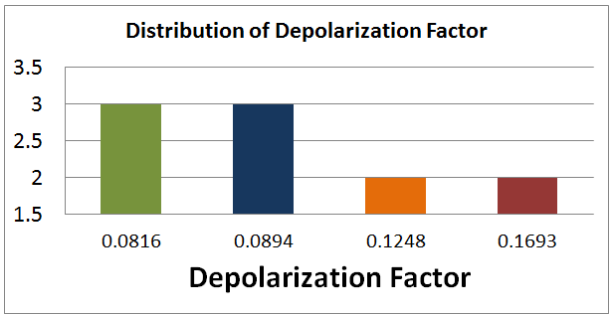

(c)

Figure 3.6: This is a histogram of distribution of involved particles of different depolarization factors in the AFM image.

So one can expect a spread of L in this range. Let us consider a weight function, $f(L)$ for the depolarization factor. For a flat smooth layer, $f(L)$ is a delta function at $L = 0$ corresponding to $z-$direction and zero value at all other values, that is between 0 to 0.99 (Fig. 3.7(b)). For a very flat oblate spheroid with very small aspect ratio, $f(L)$ would have a delta function at $L = 1 - \Delta$ (corresponding to $xy-$direction), with small value for delta. This gives values for $L_x = L_y =$

$1/2\,(1-L)$, thus resulting in two delta functions for $f(L)$. As the oblateness of spheroid increases (aspect ratio increases), Δ increases and the delta function corresponding to z-direction moves to lower values of L and the one for lateral dimension moves to higher values of L.

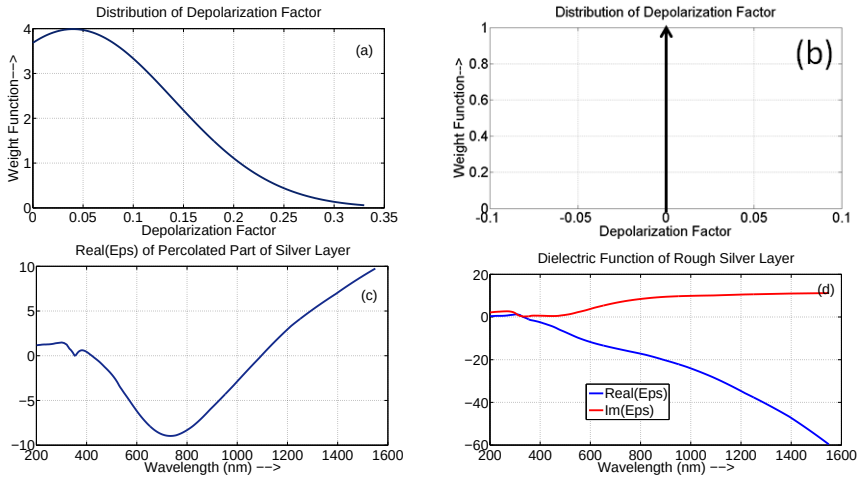

(c)

Figure 3.7: This figure summarizes the effects of a rough semi percolated silver layer with an example. (a) shows the broadening of depolarization function due to shape distribution of particles in the percolated layer. This is a weighing function that is used in calculation of effective ϵ of the group of islands. (b) is the distribution of L when silver is a flat and smooth plate. (c) shows the broadening of resonance in ϵ due to the L distribution. (d) is the effective $epsilon_{roughSilver}$ plotted for a combination of a completely uniform and completely percolated layer (roughness part) , as formulated in Eq. 3.3.

Now we try to derive this weighing function to our situation, where the particles are oblate and have a deviation from a mean value of aspect ratio as is evident from the surface morphology images. This distribution of shape can be translated into a broadening of the delta function about the mean value. Thus for the realistic case of our percolated layers, $f(L)$ can be taken as two

broadened delta functions centered at some mean values for L_z and L_{xy}. This theory is formulated below.

For modeling a percolated layer, start by considering the layer to be dielectric medium such as air or polyimide which is partially implanted with isolated silver nano inclusions [56, 66]. The inclusions are approximated as oblate spheroids (a, b, c) in (x, y, z) directions and $a = b$ and $a > c$, in line with the AFM images. Each nanospheroid has different dimensions that are random but over a mean value. Thus the depolarization factor of each spheroid is different. Effective ϵ of the entire layer is a weighted average of contributions from particles of different depolarization factors. Contribution from each nanospheroid with a depolarization factor is given by Eq. 2.5. The effective ϵ is then given by,

$$\epsilon_{percolated}(\lambda) = \int_{L_1}^{L_2} \epsilon_{eff}(\lambda; L).f(L)\, dL \tag{3.1}$$

Where $L_1\,, L_2$ are the lower and higher limits of depolarization factors in the layer, $\epsilon_{eff}(\lambda; L)$ is the contribution from a particle of a given L over λ and $f(L)$ is the weighing factor for the contribution of the particle. Since the distribution of Ls is random over a mean value, normal distribution can be used for $f(L)$.

$$f(L) = \frac{1}{\sqrt{2\pi\sigma^2}} e^{-\frac{(L-L_p)^2}{2\sigma^2}} \tag{3.2}$$

where σ^2 is the variance and L_p is the mean value of Ls. These values are the unknowns and the fitting parameters [67, 68]. These values are determined by fitting experimentally measured transmission with the transmission values calculated by substituting results of 3.1 into Eq. A.1. In this integration process, the effective dielectric function is represented as a sum of poles that are identified with resonances related to the topology of the layer. Results from this random distribution function are found to be in agreement with the approach used in [56], considering the spectral density theory. Fig. 3.7 shows an example of distribution of a set of particles in an evaporated metal layer. These plots were obtained by fitting measured data with the results from approach discussed above. Fig. 3.7 (a) displays a weight function distribution of the depolarization factor for the layer. Some fabricated samples are described in next chapter. The weighing function $f(L)$ consists of two normal

distributions corresponding to transverse and lateral dimensions. The effect of this broadening of $f(L)$ reflects in effective ϵ as a broadening of resonance, shown in Fig. 3.7(c).

3.3.2 Rough Metal Layer

In the stage before the silver layer is uniform (between 2- 15 nm), the layer is semi-percolated layer or a rough layer. To model this rough layer, we divide it into top and bottom layers, one that is uniform and is under a layer of roughness which can be modeled as a layer of nano particles in a dielectric material that is the top layer as shown in Fig. 3.8. So, the roughness layer is not treated in the same way as discussed in previous section.

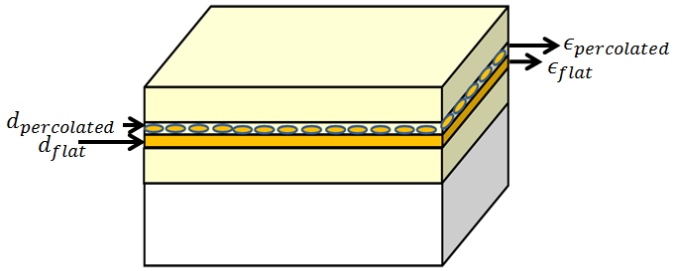

Figure 3.8: A schematic of thin film coating model used for theoretical modeling for effective dielectric function and the transmission coefficients. The a rough semi-percolated Ag layer is considered as two layers, one that is fully uniform and another that is completely percolated then each layer is treated separately.

The roughness part of the layer has an effective permittivity given by Eq. 3.1. Effective permittivity of the silver layer with the roughness included is given by using Eq. 2.14, so

$$\epsilon_{roughsilver} = \phi_1 \epsilon_{percolated} + \phi_2 \epsilon_{flat} \tag{3.3}$$

Where $\phi_{1,2} = d_{1,2}/(d_1 + d_2)$, and $d_1\, and\, d_2$ are the thicknesses of the roughness layer and flat layer respectively. This approximation is used to calculate the effective permittivity of rough silver

layers in the metal-dielectric stacks that tune λ_p. To be in the limit that the medium is homogeneous we have to go down to thicknesses of silver that are not uniform. Fig. 3.7 (d) shows an example of the result of including the roughness effects on ϵ of the silver layer. This was obtained by averaging the results given in Fig. 3.7(c) and J&C ϵ values for flat layer, with appropriate fill factors (relative thickness). Since this a weighted average, the effect of the roughness layer has substantial effect when the uniform layer is also relatively thin. But when the roughness layer is thin compared to the uniform layer the effects is negligible. Taking 20 nm layer as an example, the rms of roughness on this layer is about 4 nm and as the relative thickness is small the effects of roughness can be safely ignored.

In the next chapter, plasmonic thin film coatings are presented. The coatings consist of nano-metric silver layers separated by nano-metric layers of polyimide. Maxwell Garnett calculation of the effective dielectric function of the coating for the light propagating normal to the coating predicts a zero crossing of the real part of this function at a visible wavelength. The measured behavior of the reflectivity as a function of the wavelength is in agreement with the behavior of the reflectivity of a glass slab coated with a material with the Maxwell Garnett effective dielectric function. The concurrence of the experimental and theoretical results demonstrates that filter properties of the stack may be tuned by varying the stack geometry.

Chapter 4

Results and Discussion

Using classical theory we predict that metal layers stacked along with dielectric layers can tune plasmon wavelength λ_p to wavelengths that are not naturally available. But this tuning is significantly limited by the topological resonances occurring due to the fabrication limitations and effective medium approximation limitations. In this chapter, results from fabricated samples are shown. Samples with λ_p at different visible and near IR wavelengths are demonstrated. Two cases are studied in which 1) the predictions from classical theory are valid and 2) classical theory is contradicted due to surface irregularities. It is demonstrated that special treatment is needed for samples with relatively thin metal layers and the effects of irregularities are shown.

4.1 Comparison of Results

4.1.1 Results from Smooth layered Stacks

Samples with alternate metal and dielectric layers were fabricated using the deposition methods described in section 3.1 [69]. Five layer pairs of metal with thickness 20 nm and $PI2555$ with thickness 80 nm are deposited as shown in the schematic (Fig. 4.1). Transmission and reflection measurements are made on this sample using the set up shown in Fig. 4.2. The set up consists of a broadband source AvaLight-DHS, collimation lens, and a detector. The detector has two instruments, AvaSpec-2048 for measurements in for wavelength range of 200 nm - 900 nm and AvaSpec-NIR256-1.7 for wavelength range of 900 nm - 1600 nm.

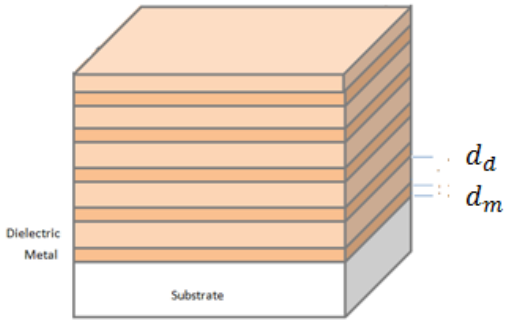

Figure 4.1: A schematic stack of layers of thin metal and dielectric layers that are smooth and uniform. This stack is used to tune λ_p in visible and near IR.

First a calibration is made on the substrate sample so that the contribution of substrate is subtracted from the actual measurement. It is to be noted that the resonance effects are not completely removed in this calibration process. After calibrating, the sample is put into the setup making sure that light in incident on coating and not the substrate, also the distances used in the calibration step must be maintained.

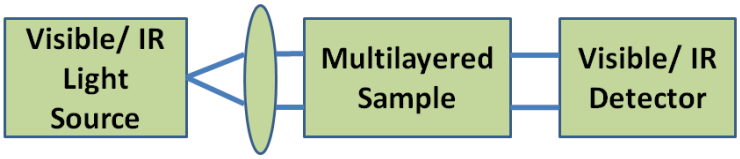

Figure 4.2: The experiment setup consists of a broadband source AvaLight-DHS (200 nm - 1800 nm), collimating lens and detectors for visible (AvaSpec-2048) and near IR for AvaSpec-NIR256-1.7.

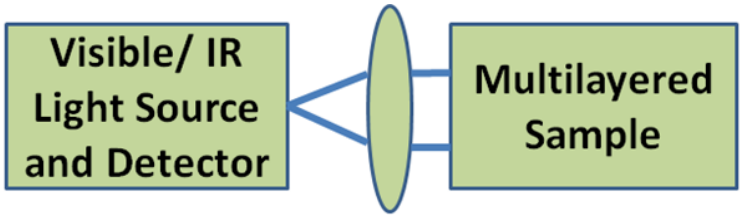

Figure 4.3: The experiment setup for reflection measurements consists of a broadband source/detector AvaLight-DHS (200 nm - 1800 nm), visible detector (AvaSpec-2048) and near IR detector for AvaSpec-NIR256-1.7 and collimating lens.

This is an example of flat and smooth silver layers, hence we can apply Eq.2.14 to calculate effective ϵ. Transmission and reflection for this set of layers can then be be computed using the Eq. A.5, Eq. A.7, Eq. A.10, Eq. A.14 and Eq. A.13. Results from this sample are shown in Fig. 4.4. Fig. 4.4(a) shows comparison of theoretically calculated transmission with the transmission measured at normal incidence and similar comparison of reflection are shown in Fig. 4.4(b). The values agree well to a good extent in transmission. However, we see significant discrepancies in reflection. The discrepancies though are for different reasons in different regions. The difference below 400 nm are attributed to the resonance of substrate glass. All the glass materials like BK-7 and sodalime have a resonance between 300 nm and 350 nm. The conflict above 400 nm is because the 1) the period thickness of layers is now close to $\lambda/4$ and 2) other reason is the delamination of layers (Fig. 4.5) due to involvement of multiple fabrication steps. This is one compelling reason to use reduced layers which serve the purpose equally well. The repeated heating of layers causes deformation of layers. This causes troubles for silver layers to adhere to the underlying layers. ϵ_{eff} of this coating is shown in Fig.4.6.

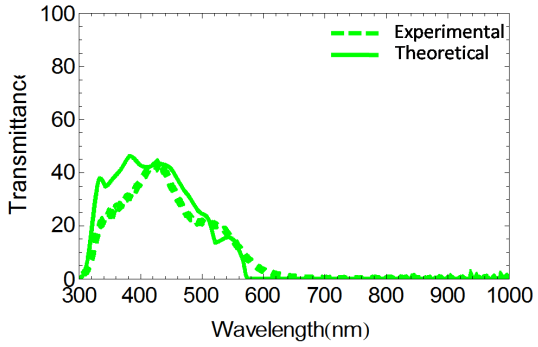

(a)

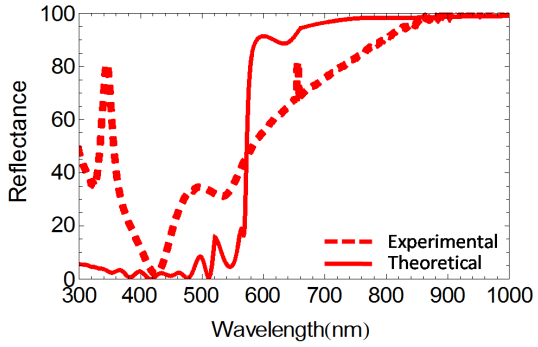

(b)

Figure 4.4: A comparison of measured and calculated transmittance and reflectance at normal incidence for the five layer Ag-PI-2555 sample with thickness of 70 nm for PI-2555 and 20 nm for silver. Transmittance peak goes to a peak of 45% indicating low loss of the coating.

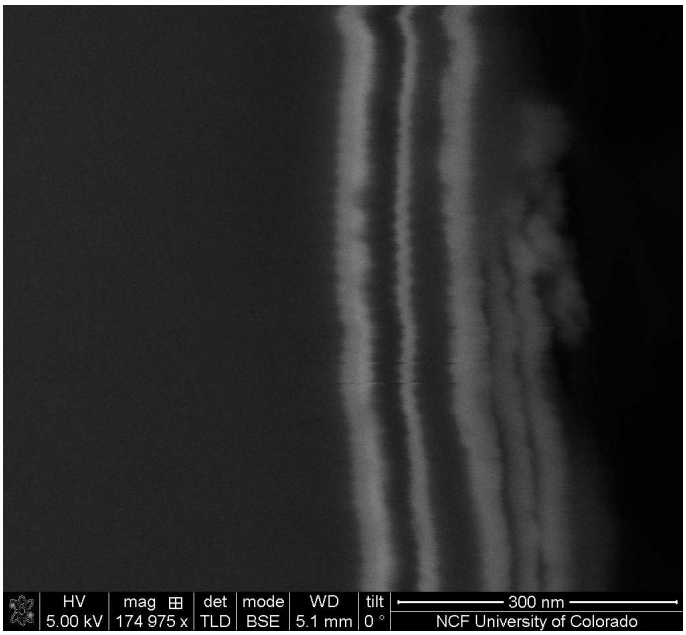

Figure 4.5: This SEM image displays the delamination of layers caused in the fabrication process due to multiple steps of spinning and heating.

This coating has λ_p at 550 nm, which is a substantial displacement of λ_p from pure silver layers $\lambda_p (= 310\, nm)$.

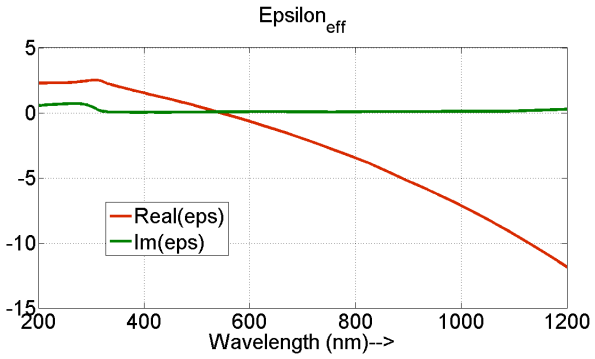

Figure 4.6: ϵ_{eff} for the coating if plotted. It has λ_p at 540 nm and $Im\{\epsilon_p\}$ is about of 0.07, thus the loss at λ_p is very small.

These coatings with smooth surfaces are easily designed using the MG approximations. All that needs to be done is to figure out a fill factor (relative thickness). Thus following equation, derived by inverting Eq. 2.14, can be used to determine the fraction of metal to make $Re\{\epsilon_{eff}\}$ zero at a given λ.

$$\frac{1}{\phi_1} = 1 - \frac{\epsilon_m(\lambda)}{\epsilon_d} \tag{4.1}$$

Fig. 4.7 shows a plot of required fraction of silver when the dielectric material is $PI2555$. To shift λ_p to higher wavelengths, ϕ should be decreased. Hence the requirement of thinner layers of metal is enforced to tune λ_p to near IR frequencies.

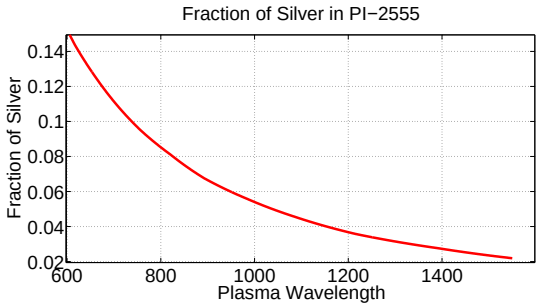

Figure 4.7: The metal fraction required to make the real part of the dielectric function of the coating zero as a function of wavelength, when the constituent layers are of $PI - 2555$(n=1) and silver.

Same kinds of results can also be obtained by using lesser number of layers at the cost of coating being more sensitive to surface quality and accuracy of thickness of layers. Also, now we use samples that have one layer of silver sandwiched between two layers of polyimide layers. This makes the fraction of metal $d_m/(d_m + 2\,d_d)$ as compared to $d_m/(d_m + d_d)$, where d_m and d_d are the thicknesses of metal and dielectric layers, respectively. This allows tuning into extended spectral range. Now combining this formula with the essential conditions for validity of effective medium

theory we can deduce a limit over which λ_p can be tuned in using these thin film stacks for given materials. we get the highest $\lambda_p$when ϕ_1 is least. If we consider maximum period thickness and minimum fraction of metal in a Ag-PI-2555 film stack, we can tune $\lambda_p$to a maximum of $3000\,nm$.

In the next samples, we will consider thinner layers of silver that do not have smooth surfaces or are percolated, to study the effects of surface topology and to compare results with the theory established in previous chapters.

4.1.2 Samples With Rough Silver Layers

Samples with thicknesses given in Table 3.1 are fabricated with one layer of silver sandwiched between two layers of $PI-2555$ layers. Transmission and reflection measurements at normal incidence are made on these samples, shown in Fig.4.8. The change in slope of transmission spectrum indicates change in $\epsilon_r$and thus tuning of λ_p. Transmission and reflection add up to 80%, indicating low scattering and absorption by these samples.

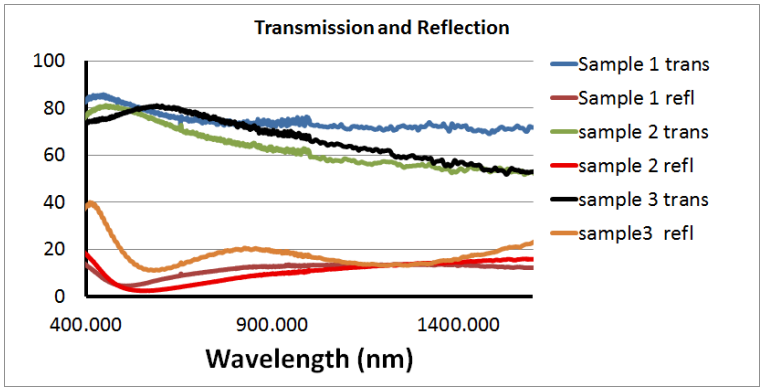

Figure 4.8: Measured transmission and reflection spectrum are plotted in this figure. The difference in slope of transmission indicates the tuning of λ_p. Transmission and reflection add up to about 80% in all cases, which is sign of low loss in the coatings.

The thickness of silver layer in sample 1 is $4.1\,nm$. At this thickness the layer is semi-percolated and fraction of metal in the layer is 0.0488. The thickness of percolated layer is $2.0\,nm$ and that of

flat part is 2.1 nm. This allows us to apply Eq.3.1 to approximate $\epsilon_{percolated}$ and then Eq. 3.3 to calculate ϵ contribution by the rough silver layer. However, the parameters for distribution function of depolarization factor for the percolated part of the silver layer are not known yet. Hence fittings of measured and theoretical transmission spectrum are made using σ and L_p for the normal distribution of Ls as parameters. The minimum root mean square is calculated to arrive at approximates for σ and L_p. Thus we calculate $\epsilon_{percolated}$ and $\epsilon_{roughsilver}$.

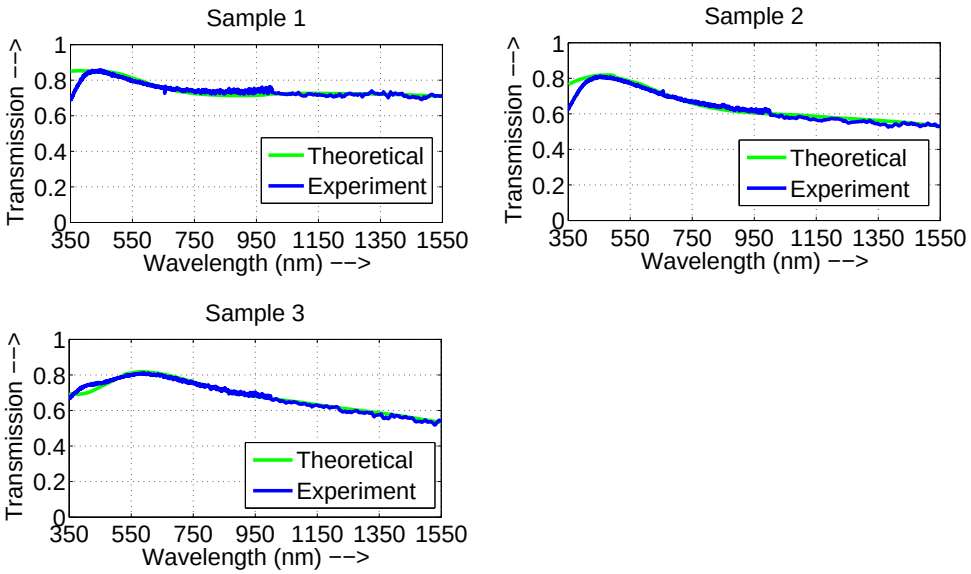

Figure 4.9: Transmission spectra for samples 1,2 and 3 were measured using Avaspec 2048 and AvaSpec NIR256-1.7 spectrometers. Transmissions were also calculated using the model shown in Fig. 3.8 and method described in previous chapter and are fitted with the measured values by varying the weighting factor parameters. The change in slope of the transmission spectra indicate the tuning of dielectric function.

The obained distribution for depolarization factor is shown in Fig 4.10. Then for $\epsilon_{coating}$, Eq.2.15 is applied by considering the layers to be 4 layers (two PI-2555 layers, one smooth Ag layer and one completely percolated layer). The parameters for the weighing function $f(L)$ are optimized

using mean square error calculated between the theoretical and measured values for transmission from 350 nm to 1600 nm. The theoretical transmission values are computed by substituting $\epsilon_{coating}$ in Eq. A.1.

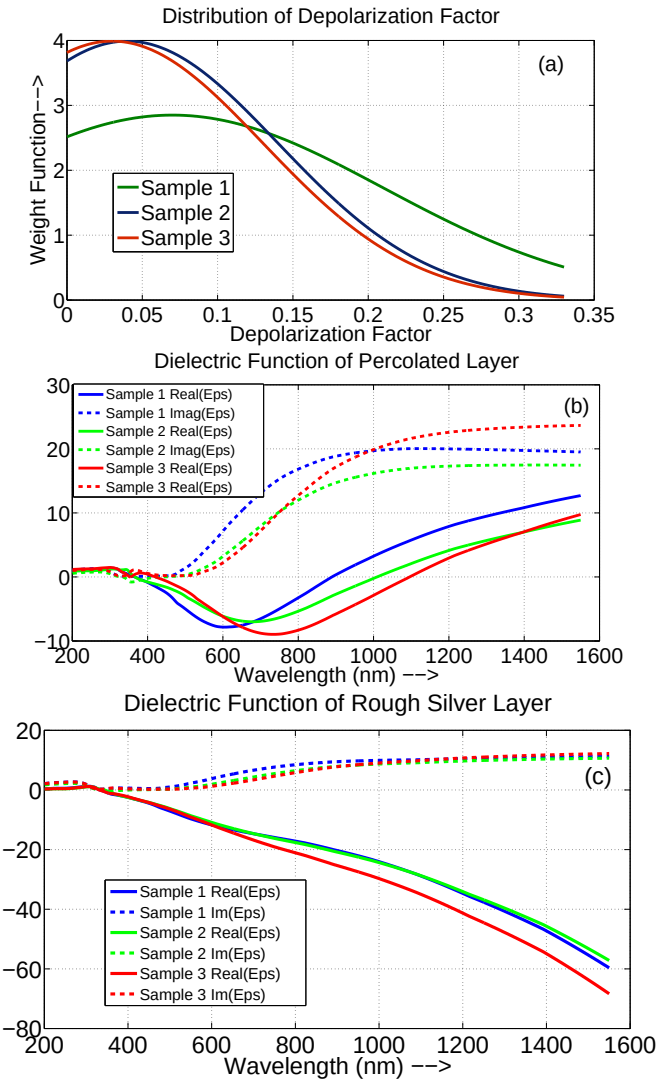

Figure 4.10: This figure plots the optical properties of rough silver layer obtained by fitting the transmission spectra for the three fabricated samples. (a) shows the distribution of depolarization function due to shape distribution of particles in the percolated layer. This is a weighing function that is used in calculation of effective ϵ of the group of islands. (b) shows $\epsilon_{percolated}$ for percolated part of the silver layers (c) is the effective $epsilon_{roughSilver}$, as formulated in Eq. 3.3.

The same procedure is repeated for samples 2 and 3 with thicknesses of metal layers 7.1 nm and 8 nm, respectively. In samples 2 and 3, the thickness of percolated parts are 3.7 nm and 3.5 nm, while the flat parts are 3.4 nm and 4.5 nm thick. The volume fraction of silver in samples 2 and 3 are 0.066 and 0.05 respectively. The distribution of L, $\epsilon_{percolated}$ and $\epsilon_{roughsilver}$ are plotted in Fig. 4.10. These depolarization factor distribution agrees well with the histogram deduced from the AFM image of silver layer. In Fig 4.10(b), we notice a notched filter behaviour but the loss is very high due to the distrubution of shapes in the percolated layer. In absence of the flat layer underlying the percolated part, the layers will be highly lossy due to scattering, but the presence of flat layer changes this behaviour significantly as the scattering due to particles reduces.

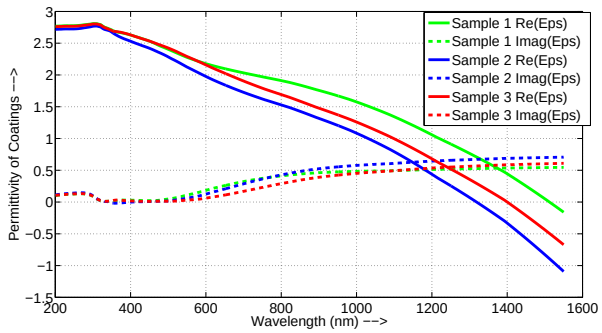

Figure 4.11: MG approximation combined with random distribution of depolarization factors (accounting for the randomness of the roughness of metal layers) is used to determine the dielectric function, $\epsilon_{coating}(\lambda)$ of samples 1,2 and 3. The samples have different fractions of metal in the three-layered sandwich coatings. In this figure, shift in λ_0 is evident and so is the change in dielectric function.

Fig. 4.11 shows the tuning of $\epsilon_{coating}$ for samples 1, 2 and 3. Samples 1, 2 and 3 have λ_p are 1510 nm, 1320 nm, *and* 1400 nm. As the fraction of metal in these samples changes, λ_p is shifted. To understand the changes roughness brings to these coatings, I plotted the ideal cases when these

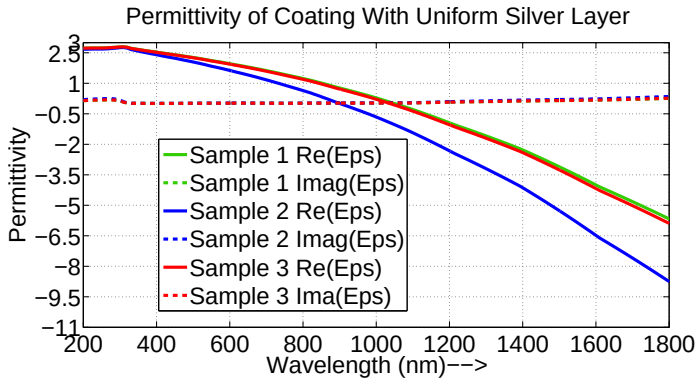

Figure 4.12: For the samples with semi-percolated layers fabricated and measured above, if the layers were not percolated we can directly apply Eq.2.14. If it were possible, λ_p in each case would be as shown in this figure. Comparing these with actual results show that the effect of percolated layer is to shift λ_p to higher wavelengths, but not very drastic changes are observed in the properties of the coatings.

thin layers have uniform surfaces. Fig. 4.12 shows the results plotted using the 2.14 for samples 1, 2 and 3 (that is, using the same thicknesses). The ideal samples 1, 2 and 3 would have had λ_p at $1060\,nm$, $1050\,nm$ and $900\,nm$, respectively. The difference between the rough layer case is that λ_p is shifted to higher wavelengths for rough layers, but no new features are introduced. Having said that, the shift in λ_p cannot be ignored, as it has its own share of advantages and disadvantages. Infact the limitations in fabrication process of the silver layers actually works in our favour in allowing us to move λ_p to higher wavelengths.

4.2 Summary

The stacks of metal-dielectric layer have a huge potential in various applications. One of the most popular applications after the high quality mirror would be for tuning the plasma wavelength over spectral range in visible and near-IR when the dimensions of the layers are smaller than the wavelength of operation. An inhomogeneous medium is seen as a homogeneous layers when the particle metal nanostructure dimensions are smaller than $\lambda/4$. An extra condition for validation of effective medium theory has been established based on comparisons of results from theory and experiments. In case of multilayers along with the metal thickness, the metal-dielectric period

thickness should also be smaller than $\lambda/4$. Silver is the best choice for these applications in visible because it has lower loss than others, which is reflected in its $Im\{eps\}$.

To obtain λ_p in near IR regions, the fraction of metal, in other words the thickness of metal layer should be smaller than the limit where one can get smooth flat layers. Hence such semi-percolated and percolated layers were studied in detail. The percolated layers have random distribution of particle shapes involved. These particles have different contribution to the optical properties of the medium defined by the depolarization factor. Depolarization factor for various shapes with varied symmetry are studied, for example spheres, ellipsoids and cubes. The depolarization factors indicate the occurrences of resonance in the medium. For the percolated layers, a normal distribution based weighing function is defined for the depolarization factor. This statistical model is combined with Maxwell Garnett approximation to calculate the effective properties of the percolated layer. Maxwell Garnett gives reasonably Good results when the metal fraction is below a certain threshold. Hence the effects of these non uniform layers on the entire coating was studied.

Fabricated layered structures with alternate thin layers of thickness far less than a quarter of wavelength of incident light were studied. Measurements of transmittance of light incident normal to the plane of layers are made. Dielectric functions were obtained using Maxwell Garnett theory for smooth layers and an extended model based on the irregularities of the surfaces was used for semi-percolated layers. Even in the case of percolated layers, the tuning of λ_p was successfully accomplished. The effect of roughness was only seen as a shift in λ_p into higher wavelengths and is actually advantageous if the purpose is to tune λ_p to higher wavelength. Thus tuning capabilities of thin film stacks with low loss are verified experimentally and theoretically. However, proper characterization of these layers is very critical in this procedure for the structure to be designed well and to be used in practical applications. The statistical model, presented in this thesis, serves this purpose very effectively while characterizing the effects of roughness of thin silver films on optical properties.

Bibliography

[1] R. Zia, J. A. Schuller, A. Chandran, and M. L. Brongersma, "Plasmonics: The next chip-scale technology," Materials Today, vol. 9(7-8), pp. 20–27, 2006.

[2] E. Ozbay, "Plasmonics: Merging photonics and electronics at nanoscale dimensions," Science, vol. 311, pp. 189–193, 2006.

[3] S. A. Maier and H. A. Atwater, "Plasmonics: Localization and guiding of electromagnetic energy in metal/dielectric structures," Journal of Applied Physics, vol. 98, pp. 011 101–1–011 101–10, 2005.

[4] W. L. Barnes, A. Dereux, and T. W. Ebbesen, "Surface plasmon subwavelength optics," Nature, vol. 424, pp. 824–830, 2003.

[5] M. Silveirinha, A. Alu, B. Edwards, and N. Engheta, "Overview of theory and applications of epsilon-near-zero materials," Nanoengineering: Fabrication, Properties, Optics, and Devices SPIE, vol. 5515, pp. 180–186, 8 October 2004.

[6] K. Lewotsky, "The promise of plasmonics," July 2007.

[7] M. G. Silveirinha and A. Alu, "Theory of supercoupling, squeezing wave energy, and field confinement in narrow channels and tight bends using epsilon near-zero metamaterials," Departmental Papers ESE, March 2007.

[8] H. M. Hiep, T. Endo, K. Kerman, M. Chikae, D. Kim, S. Yamamura, Y. Takamura, and E. Tamiya, "A localized surface plasmon resonance based immunosensor for the detection of casein in milk," Sci. Technol. Adv. Mater., vol. 8, p. 331, 2007.

[9] HDMicroSystems, "Product bulletin: Pi2525, pi2555, pi2556 and pi2574," September 2009.

[10] S. Assefa, F. Xia, and A. Vlasov, Y., "Reinventing germanium avalanche photodetector for nanophotonic on-chip optical interconnects," Nature, vol. 464, p. 7285, 2010.

[11] Z. Liu, M. D. Thoreson, A. V. Kildishev, and V. M. Shalaev, "Translation of nanoantenna hot spots by a metal-dielectric composite superlens," Appl. Phys. Lett., vol. 95, no. 3, p. 033114, 2009.

[12] A. Alu, A. Salandrino, and N. Engheta, "Negative effective permeability and left-handed materials at optical frequencies," Opt. Express, vol. 14, pp. 1557 – 1567, 2006.

[13] U. K. Chettiar, A. V. Kildishev, T. A. Klar, and V. M. Shalaev, "Negative index metamaterial combining magnetic resonators with metal films," vol. 14.

[14] L. Menon, W. T. Lu, A. L. Friedman, S. P. Bennett, D. Heiman, and S. Sridhar, "Negative index metamaterials based on metal-dielectric nanocomposites for imaging applications," Appl. Phys. Lett., vol. 93, p. 123117, 2008.

[15] M. Silveirinha, A. Alu, and N. Engheta, "Parallel-plate metamaterials for cloaking structures," Phys. Rev. E, vol. 75, no. 3, March 2007.

[16] B. Schwartz and R. Piestun, "Waveguiding light in air with ultralow index materials," in Nanoengineering: Fabrication, Properties, Optics, and Devices SPIE, vol. 5515, 8 October 2004, pp. 180 – 186.

[17] S. Liao, "Rf shielding effectiveness and light transmission of copper or silver film coating on plastic substrate," IEEE Transactions on Electromagnetic Compatibility, EMC, vol. 18, no. 4, pp. 148 – 153, 1976.

[18] W. Cai, U. K. Chettiar, A. V. Kildishev, and V. M. Shalaev, "Optical cloaking with metamaterials," vol. 1.

[19] A. Alu and N. Engheta, "Achieving transparency with plasmonic and metamaterial coating," Phys. Rev. E, vol. 72, 2005.

[20] J. B. Pendry, "Negative refraction makes a perfect lens," Phys. Rev. Lett., vol. 85, pp. 3966–3969, 2000.

[21] S. Ramakrishna, J. B. Pendry, M. C. K. Wiltshire, and W. J. Stewart, "Imaging the near-field," J. Mod. Optics, vol. 50, no. 9, pp. 1419 – 1430, 15 June 2003.

[22] Y. Xiong, v. Liu, S. Durant, H. Lee, C. Sun, and X. Zhang, "Tuning the far-field superlens: from uv to visible," vol. 15.

[23] A. Alu, M. Silveirinha, A. Salandrino, and N. Engheta, "Epsilon- near-zero metamaterials and electromagnetic sources: Tailoring the radiation phase patterns," Phys. Rev. B, vol. 75, no. 15, 15 April 2007.

[24] R. Ziolkowski and E. Heyman, "Wave propagation in media having negative permittivity and permeability," Phys. Rev. E, vol. 64, p. 056625, 2001.

[25] Y. K. Choi, Y. Ha, J. Kim, and K. Park, H. Y.and Kim, "Antireflection film in one-dimensional metallo-dielectric photonic crystals," Optics Communication, vol. 230, February, 2004.

[26] S. Enoch, G. Tayeb, P. Sabouroux, N. GuÃ©rin, and P. Vincent, "A metamaterial for directive emission," Phys. Rev. Lett., vol. 89, p. 3902, 2002.

[27] V. P. Duggal and V. P. Nagpal, "Size effect in thin single crystal silver films," Appl. Phys. Lett., vol. 13, p. 206, 1968.

[28] A. Kawabata and R. Kubo, "Electronic properties of fine metallic particles. ii. plasma resonance absorption," J. Phys. Soc. Jpn., vol. 21, p. 1765, 1966.

[29] L. P. Gor'kov and G. M. Eliashberg, "Minute metallic particles in an electromagnetic field," Sov. Phys. JETP, vol. 21, p. 940, 1965.

[30] U. Kreibig and M. Vollmer, Minute metallic particles in an electromagnetic field. Springer-Verlag: Berlin, Heidelberg, 1995, ch. Optical properties of metal clusters.

[31] G. Mie, "Beitrage zur optik truber medien, speziell kolloidaler metallosungen," Annalen Der Physik, vol. 25, 1908.

[32] P. Drude, "Zur elektonentheorie der metalle," Annalen der Physik, vol. 306(3), pp. 566–613, 1900.

[33] ——, "Zur elektonentheorie der metalle ii. teil. galvanomagnetische und thermoagnitische effekte," Annalen der Physik, vol. 308(11), pp. 369–402, 1900.

[34] C. F. Bohren and D. R. Huffman, Absorption and Scattering of Light by Small Particles. Wiley, New York,, 1983.

[35] P. Johnson and R. Christy, "Optical constants of nobel metals," Phys. Rev. B, vol. 6, no. 12, pp. 4370–4379, December 1972.

[36] E. D. Palik, Handbook of Optical Constants of Solids. Academic Press, Boston, 1985, pp. 12–49.

[37] M. J. Weber, Handbook of optical materials, 3rd ed. CRC: New York, 2003, pp. 12–49.

[38] V. P. Drachev, U. K. Chettiar, A. V. Kildishev, H. Yuan, W. Cai, and V. M. Shalaev, "The ag dielectric function in plasmonic metamaterials," Opt. Express, vol. 515, no. 16, pp. 1186–1195, 2008.

[39] R. Landauer, "Electrical conductivity in inhomogeneous media," AIP Conf. Proc., vol. 40, pp. 2–45, 2010.

[40] V. M. Shalaev, Nonlinear Optics of Random Media: Fractal Composites and Metal-Dielectric Films. Springer,Berlin, 2000, pp. 12–49.

[41] U. Chettiar, P. Nyga, M. Thoreson, A. Kildishev, V. Drachev, and V. Shalaev, "Fdtd modeling of realistic semicontinuous metal films," vol. 100.

[42] R. Nielsen, M. Thoreson, W. Chen, A. Kristensen, J. Hvam, V. Shalaev, and A. Boltasseva, "Toward superlensing with metalï¿œdielectric composites and multilayers," vol. 100.

[43] W. Chen, M. D. Thoreson, A. V. Kildishev, and V. M. Shalaev, "Fabrication and optical characterizations of smooth silver-silica nanocomposite films," vol. 7.

[44] S. Bosch, J. Ferrï¿œ-Borrull, N. Leinfellner, and A. Canillas, "Effective dielectric function of mixtures of three or more materials: a numerical procedure for computations," vol. 453.

[45] A. Sihvola, Electromagnetic mixing formulas and applications. The Institution of Electrical Engineers, London, 1999.

[46] B. DAG, "Berechnung verschiedener physikalischer konstanten von heterogenen substanzen. i. dielektrizitï¿œatskonstanten und leitfï¿œahigkeiten der mischkï¿œorper ausisotropen substanzen," vol. 24.

[47] H. Wallen, H. Kettunen, and A. Sihvola, Metamaterials and plasmonics: Fundamentals,Modelling,Applications. Springer, 2008, ch. Mixing Formulas and Plasmonic Composites.

[48] J. C. Maxwell Garnett, "Colours in metal glasses and in metallic films," Phil. Trans. R. Soc. Lond. A, vol. 203, pp. 385–420, 1904.

[49] J. C. Maxwell-Garnett, "Colours in metal glasses, in metallic films, and in metallic solutions," Transactions of the Royal Society of London, vol. 205, pp. 237–288, 1906.

[50] O. F. Mossotti, "Discussione analitica sul'influenza che l'azione di un mezzo dielettrico ha sulla distribuzione dell'elettricita alla superficie di piu corpi elettrici disseminati un eso," Mem. Mat. Fis. della Soc. Ital. di Sci. in Modena, vol. 24, pp. 49–74, 1850.

[51] L. Lorentz, "Uber die refraktionskonstante," Ann. Phys. Chem., vol. 11, p. 70, 1880.

[52] F. Galeener, "Submicroscopic-void resonance: The effect of internal roughness on optical absorption," vol. 27.

[53] E. M. Lifshitz, L. D. Landau, and L. P. Pitaevskii, Electrodynamics of Continuous Media, 2nd ed. Butterworth-Heinemann, 1984, ch. Electrostatics of Conductors, pp. 19–25.

[54] J. A. Stratton, Electromagnetic Theory, 1st ed. McGraw-Hill Book Company, 1941, ch. III, pp. 213–218.

[55] R. W. Cohen, G. D. Cody, M. D. Coutts, and B. Abeles, "Optical properties of granular silver and gold films," Phys. Rev. B, vol. 8, pp. 3689–3701, 15 October 1973.

[56] J. Sancho-Parramon, V. Janicki, and H. Zorc, "On the dielectric function tuning of random metal-dielectric nanocomposites for metamaterial applications," Opt. Express, vol. 18, no. 26, pp. 26 915–26 928, 2010.

[57] C. G. Granqvist and O. Hunderi, "Conductivity of inhomogeneous materials: Effective medium theory with dipole-dipole interaction," vol. 18.

[58] R. Fuchs, "Theory of the optical properties of ionic crystal cubes," vol. 11.

[59] A. Mejdoubi and C. Brosseau, "Finite-element simulation of the depolarization factor of arbitrarily shaped inclusions," Magnetics, IEEE Transactions on, vol. 44, no. 6, pp. 1142 – 1145, June 2008.

[60] M. Rytov, "Electromagnetic properties of a finely stratified medium," Sov. Phys. JETP, vol. 2, pp. 466–475, 1956.

[61] X. Sun, R. Honga, H. H., Z. Fan, and J. Shaoa, "Thickness dependence of structure and optical properties of silver films deposited by magnetron sputtering," Thin Solid Films, vol. 515, no. 17, pp. 6962–6966, 13 June 2007.

[62] X. Li and F. Zhuang, "Multilayered structures with high subwavelength resolution based on the metal-dielectric composites," J. Opt. Soc. Am. A, vol. 26, no. 12, pp. 2521–2525, 2009.

[63] L. Shi and L. Gao, "Subwavelength imaging from a multilayered structure containing interleaved nonspherical metal-dielectric composites," Phys. Rev. B, vol. 77, p. 195121, 2008.

[64] C. T. Sullivan and A. Husain, "Optical computing and nonlinear materials," SPIE Proc., vol. 881, p. 172, 1988.

[65] K. Hinsen and B. U. Felderhof, "Dielectric constant of a suspension of uniform spheres," vol. 46.

[66] D. Bergman, "The dielectric constant of a composite material-a problem in classical physics," Physics Reports, vol. 43, no. 9, pp. 377–407, 1978.

[67] A. R. Day and M. F. Thorpe, "The spectral function of composites: the inverse problem," vol. 11.

[68] A. R. Day, A. R. Grant, A. J. Sievers, and M. F. Thorpe, "Spectral function of composites from reflectivity measurements," vol. 84.

[69] J. Karri and A. Mickelson, "Silver dielectric stack with near-zero epsilon at a visible wavelength," Nanotechnology Materials and Devices Conference, 2009. NMDC '09. IEEE, pp. 148 – 153, 2-5 June 2009.

[70] M. Born and E. Wolf, Principles of Optics, 17th ed. Cambridge University Press, 1999, ch. Basic Properties of Electromagnetic Field, pp. 58–71.

[71] F. Abeles, "Recherche sur la propagation des ondes electromagnï¿œtiques sinusoidales dans les milieux stratifiï¿œs. applications aux couches minces," Ann. De. Physique, vol. 5, pp. 596–640 and 706ï¿œ782, 1950.

[72] H. A. Macleod, Thin Film Optical Filters, 3rd ed. Taylor and Francis, 2001, ch. Basic theory, pp. 12–49.

Appendix A

Transmission and Reflection From Multilayers

A.1 Fresnel Coefficients For Single Interface

In this work, multiple layers of metal and dielectric were used to solve for the problem of achieving low loss plasmonic materials and for tuning the plasmon wavelength. Theoretical predictions were compared with experimental results. This was implemented by measurements of transmission. This section briefs the theoretical calculations of the transmission and reflection of stacked multiple layers.

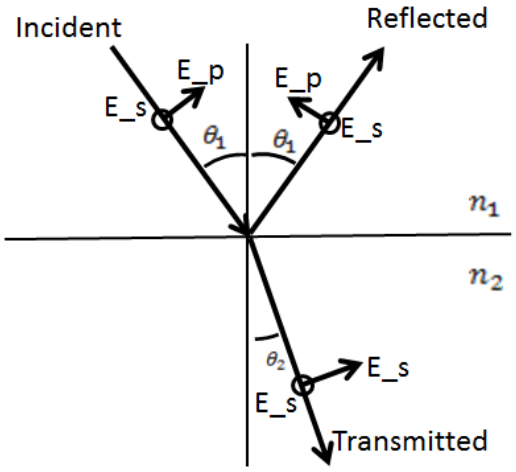

Figure A.1: This figure shows a single interface between two semi-infinite medium. When a wave is incident on an interface there is a transmitted and reflected wave.

To start with, consider two different semi infinite media sharing a boundary as in Fig. A.1. When a plane wave is incident on the interface, it is split into reflected and transmitted wave. If

one of the media is conductive, then some of the incident light is absorbed. Snell's law gives the direction of the transmitted wave. Now for amplitude of the transmitted and reflected waves, we use Fresnel's relations. Fresnel relations define transmission and reflection coefficients for parallel and perpendicular polarizations as

$$t_{\perp} = \frac{2cos\theta_1/\eta_1}{(cos\theta_1/\eta_1 + cos\theta_2/\eta_2)} \tag{A.1}$$

$$t_{||} = \frac{2cos\theta_1/\eta_2}{(cos\theta_1/\eta_1 + cos\theta_2/\eta_2)} \tag{A.2}$$

$$r_{\perp} = \frac{(cos\theta_1/\eta_1 - cos\theta_2/\eta_2)}{(cos\theta_1/\eta_1 + cos\theta_2/\eta_2)} \tag{A.3}$$

$$r_{||} = \frac{(cos\theta_1/\eta_1 - cos\theta_2/\eta_1)}{(cos\theta_1/\eta_2 + cos\theta_2/\eta_1)} \tag{A.4}$$

η_i , $i = 1, 2$ are the impedances of the two media, $\eta = \sqrt{\mu_r/\epsilon_r}$. $\theta_2$is given by Eq.1.17. In optical frequencies, $\mu_r = 1$ and using $n = \sqrt{\epsilon_r}$, and the Fresnel equations simplify to

$$t_{\perp} = \frac{2n_1cos\theta_1}{(n_1cos\theta_1 + n_2cos\theta_2)} \tag{A.5}$$

$$t_{||} = \frac{2n_1cos\theta_1}{(n_2cos\theta_1 + n_1cos\theta_2)} \tag{A.6}$$

$$r_{\perp} = \frac{(n_1cos\theta_1 - n_2cos\theta_2)}{(n_1cos\theta_1 + n_1cos\theta_2)} \tag{A.7}$$

$$r_{||} = \frac{(n_2cos\theta_1 - n_1cos\theta_2)}{(n_2cos\theta_1 + n_1cos\theta_2)} \tag{A.8}$$

The transmission and reflection magnitude are thus given by

$$T_{\perp/||} = |t_{\perp/||}|^2$$

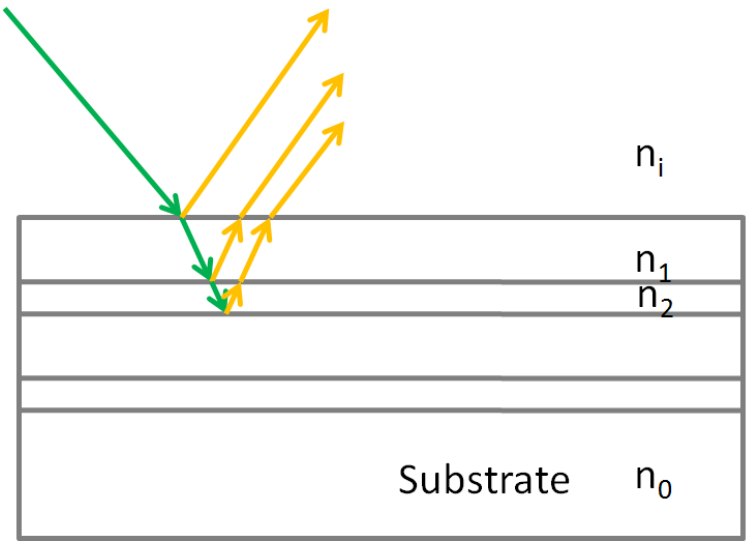

Figure A.2: A multilayered system is demonstrated. At each interface there is transmittance and reflectance. All the transmissions and reflections add coherently.

$$R_{\perp/||} = |r_{\perp/||}|^2$$

A.2 Fresnel Coefficients For Multiple Layers

For a system with multiple layers, at each interface there is reflection and transmission. These transmission and reflected waves interfere and give a net effect dependent on wavelength. We can use a characteristic matrix for each layer. And for multiple layers, the product of the characteristic matrices of each layer gives reflection and transmission coefficients of the stratified medium[70, 71, 72].

$$M = M_1.M_2....M_n \tag{A.9}$$

M_i is given as,

$$M_i = \begin{bmatrix} m_{11} & m_{12} \\ m_{21} & m_{21} \end{bmatrix} = \begin{bmatrix} cos(kn_l l_l cos\theta_l) & -\frac{i}{p_l} sin(kn_l l_l cos\theta_l) \\ -i\, p_l\, sin(kn_l l_l cos\theta l_1) & cos(kn_l l_l cos\theta_l) \end{bmatrix} \tag{A.10}$$

where n_l, l_l, , $\theta_l$are the refractive index and thickness of the layer and the angle of propagation of light beam in the layer. $k = 2\,\pi/\lambda$ is the wave vector of the light beam. θ_l is given by Snell's law Eq[]. For a s-polarized incident plane wave, $p_l = \sqrt{\frac{\epsilon_l}{\mu_l}}\,cos(\theta_l)$ and for p-polarized incident plane wave, $p_l = \sqrt{\frac{\mu_l}{\epsilon_l}}cos(\theta_l)$. To get the reflection and transmission coefficients for plane waves, we can use,

$$r = \frac{(m_{11} + p_0 m_{12})p_i - (m_{21} + p_0 m_{22})}{(m_{11} + p_0 m_{12})p_i + (m_{21} + p_0 m_{22})} \tag{A.11}$$

$$t = \frac{2p_i}{(m_{11} + p_0 m_{12})p_i + (m_{21} + p_0 m_{22})} \tag{A.12}$$

Again, $p_{i/0} = \sqrt{\frac{\epsilon_{i/0}}{\mu_{i/0}}}\,cos(\theta_{i/0})$ and for p-polarized incident plane wave, $p_{i/0} = \sqrt{\frac{\mu_{i/0}}{\epsilon_{i/0}}}\,cos(\theta_{i/0})$, i is for the input medium and 0 is for the output medium . In the above equations, n_i,n_0 are the refractive indices of incident medium and the output medium or substrate, respectively. θ_i,θ_0 are the incident and refraction angles in the incident medium and the substrate respectively. Now, reflectivity and transmittance of the coating are given by

$$R_s = |r_s|^2 \tag{A.13}$$

$$T_s = |t_s|^2 \frac{p_0}{p_l} \tag{A.14}$$

The transmittance has to be normalized with the refractive index of the substrate to account for the fact that in the derivation of these formulas output medium is considered as infinite but the transmission measurement is made in air.

For normal incidence in a non-magnetic medium, $\theta = 0$ thus the formulas A.11 and A.12 reduce to

$$r = \frac{(m_{11} + n_0 m_{12})n_i - (m_{21} + n_0 m_{22})}{(m_{11} + n_0 m_{12})n_i + (m_{21} + n_0 m_{22})} \tag{A.15}$$

$$t = \frac{2n_i}{(m_{11} + n_0 m_{12})n_i + (m_{21} + n_0 m_{22})} \tag{A.16}$$

and the characteristic matrix becomes

$$\begin{bmatrix} m_{11} & m_{12} \\ m_{21} & m_{21} \end{bmatrix} = \begin{bmatrix} cos(kn_1l_1) & -i\frac{1}{n_1}sin(kn_1l_1) \\ -in_1sin(kn_1l_1) & cos(kn_1l_1) \end{bmatrix} \tag{A.17}$$